AGU PUBLICATIONS

JGR

Journal of Geophysical Research: Atmospheres

RESEARCH ARTICLE
10.1002/2014JD021913

Key Points:
- Atmospheric marine aerosol particles separated into four organic mass types
- Generated and atmospheric primary marine aerosols have similar compositions
- Organic composition of primary marine aerosol is linked to seawater organics

Supporting Information:
- Readme
- Sections 7.1–7.7, Tables S1–S4, and Figures S1 and S2

Correspondence to:
L. M. Russell,
lmrussell@ucsd.edu

Citation:
Frossard, A. A., L. M. Russell, S. M. Burrows, S. M. Elliott, T. S. Bates, and P. K. Quinn (2014), Sources and composition of submicron organic mass in marine aerosol particles, *J. Geophys. Res. Atmos.*, *119*, 12,977–13,003, doi:10.1002/2014JD021913.

Received 21 APR 2014
Accepted 17 OCT 2014
Accepted article online 21 OCT 2014
Published online 26 NOV 2014

Sources and composition of submicron organic mass in marine aerosol particles

Amanda A. Frossard[1,2], Lynn M. Russell[1], Susannah M. Burrows[3], Scott M. Elliott[4], Timothy S. Bates[5,6], and Patricia K. Quinn[6]

[1]Scripps Institution of Oceanography, University of California, San Diego, La Jolla, California, USA, [2]Now at Department of Chemistry, University of California, Berkeley, California, USA, [3]Atmospheric Science and Global Change Division, Pacific Northwest National Laboratory, Richland, Washington, USA, [4]Los Alamos National Laboratory, Los Alamos, New Mexico, USA, [5]Joint Institute for the Study of the Atmosphere and Oceans, University of Washington, Seattle, Washington, USA, [6]Pacific Marine Environmental Laboratory, NOAA, Seattle, Washington, USA

Abstract The sources and composition of atmospheric marine aerosol particles (aMA) have been investigated with a range of physical and chemical measurements from open-ocean research cruises. This study uses the characteristic functional group composition (from Fourier transform infrared spectroscopy) of aMA from five ocean regions to show the following: (i) The organic functional group composition of aMA that can be identified as mainly atmospheric primary marine (ocean derived) aerosol particles (aPMA) is 65 ± 12% hydroxyl, 21 ± 9% alkane, 6 ± 6% amine, and 7 ± 8% carboxylic acid functional groups. Contributions from photochemical reactions add carboxylic acid groups (15%–25%), shipping effluent in seawater and ship emissions add additional alkane groups (up to 70%), and coastal or continental emissions mix in alkane and carboxylic acid groups. (ii) The organic composition of aPMA is nearly identical to model-generated primary marine aerosol particles from bubbled seawater (gPMA, which has 55 ± 14% hydroxyl, 32 ± 14% alkane, and 13 ± 3% amine functional groups), indicating that its overall functional group composition is the direct consequence of the organic constituents of the seawater source. (iii) While the seawater organic functional group composition was nearly invariant across all three ocean regions studied and the ratio of organic carbon to sodium (OC/Na^+) in the gPMA remained nearly constant over a broad range of chlorophyll *a* concentrations, the gPMA alkane group fraction appeared to increase with chlorophyll *a* concentrations ($r = 0.66$). gPMA from productive seawater had a larger fraction of alkane functional groups (42 ± 9%) compared to gPMA from nonproductive seawater (22 ± 10%), perhaps due to the presence of surfactants in productive seawater that stabilize the bubble film and lead to preferential drainage of the more soluble (lower alkane group fraction) organic components. gPMA has a hydroxyl group absorption peak location characteristic of monosaccharides and disaccharides, where the seawater organic mass hydroxyl group peak location is closer to that of polysaccharides. This may result from the larger saccharides preferentially remaining in the seawater during gPMA and aPMA production.

1. Introduction

Atmospheric marine aerosol particles (aMA) influence cloud microphysical processes in marine regions [*de Leeuw et al.*, 2011], in addition to scattering and absorbing solar radiation [*Erlick et al.*, 2001] in the marine boundary layer (MBL). The aMA directly scatter incoming solar radiation contributing to a cooling of the surface. Organic constituents that mixed with sea salts in aMA can reduce this cooling effect [*Randles et al.*, 2004]. The aMA also provide cloud condensation nuclei (CCN) over the open ocean [*Clarke et al.*, 2006]. Determining the composition and the sources of the organic fraction of aMA is important for understanding the degree to which aMA contributes to the current and future aerosol climate forcing [*Randles et al.*, 2004].

Primary marine aerosol particles (PMA), also referred to as nascent sea spray aerosol (Table 1), are defined as those produced directly at the ocean surface, prior to undergoing chemical reactions or condensational growth in the atmosphere. Breaking waves at the sea surface trap air that then rises as bubbles. At the sea surface, these bubbles burst, and their film produces submicron aerosol particles [*Blanchard and Woodcock*, 1980] that contain organic components, in addition to sea salt [*Blanchard*, 1964]. The organic mass (OM) fraction of aMA has been investigated by numerous analytical methods, each of which has provided an incomplete characterization of aMA OM composition and its sources (Table 2). For example, some studies

Table 1. Definitions of Marine Aerosol and Relevant Seawater Terminology

Term	Definition	Previous Related Usage	Additional Information
Marine Aerosol			
aMA	atmospheric marine aerosol particles	this study	see references in Table 2
PMA	primary marine aerosol; particles emitted directly from the sea surface	*O'Dowd and De Leeuw* [2007] and *Long et al.* [2014]	sea spray aerosol (SSA) [*Quinn et al.*, 2014, and elsewhere]
gPMA	model-generated primary marine aerosol	this study	nascent SSA [*Quinn et al.*, 2014], bubble-mediated marine primary organic aerosol [*Facchini et al.*, 2008a], and model-generated PMA (mPMA) [*Long et al.*, 2014]
Four aMA OM Types[a]			
aPMA	atmospheric PMA particles	this study	contains >70% PMA from seawater and <30% from other sources
CMA	aPMA enriched with secondary carboxylic acid marine aerosol particles	this study	includes 50–70% aPMA and contains >10% carboxylic acid groups by mass
SMA	shipping-influenced marine aerosol particles	this study	includes >30% fuel combustion sources in addition to <70% aPMA
MMA	mixed marine aerosol particles	this study	includes 20–40% each of aPMA, SMA, and CMA
Seawater			
Productive	biologically productive seawater in eutrophic conditions	*Quinn et al.* [2014]	high biological activity (HBA) [*O'Dowd et al.*, 2004]
Nonproductive	biologically nonproductive seawater in oligotrophic conditions	*Quinn et al.* [2014] (oligotrophic)	low biological activity (LBA) [*O'Dowd et al.*, 2004]

[a]Can contain contribution of <30% from other OM types.

have focused on the water-soluble or water-insoluble organic carbon (WSOC and WIOC, respectively) content of submicron aerosol particles. An enrichment in WIOC relative to WSOC has been associated with PMA OM, which was separated from nonmarine aerosol based on surface wind direction, wind speed, black carbon concentration, and particle number concentrations at a coastal ground site in Ireland influenced by aerosol from the northeastern Atlantic [*O'Dowd et al.*, 2004]. Measurements of vertical concentration gradients of submicron WIOC at this site were used to infer that measured WIOC was PMA [*Ceburnis et al.*, 2008]. At that same site, *Ovadnevaite et al.* [2011] measured the mass spectral signature of nonrefractory aMA from the North Atlantic and classified the hydrocarbon-like components as PMA, based on their similarity to water-insoluble organic mass (WIOM) [*O'Dowd et al.*, 2004]. In addition, the collection and extraction of filter samples have enabled the quantification of low molecular weight (LMW) saturated fatty acids in aMA from the North Pacific, which, based on correlations with sea salt, were found to be associated with PMA [*Mochida et al.*, 2002]. *Leck and Bigg* [2008] used electron microscopy to identify morphological behavior that is consistent with particles containing polymer gels in air masses collected downwind from the outer edge of the Great Barrier Reef, Australia. Studies in the Arctic have associated the organic fraction of PMA with biopolymeric hydrogels [*Orellana et al.*, 2011; *Bigg and Leck*, 2008; *Leck and Bigg*, 2005]. Other studies have characterized PMA OM by its functional group composition: in the North Atlantic and Arctic Oceans, submicron aMA OM was identified as largely PMA based on correlation to submicron Na^+ and wind speeds, as well as back trajectories, and was observed to contain carbohydrate-like (saccharide) content [*Hawkins and Russell*, 2010; *Russell et al.*, 2010].

In addition to PMA generated from seawater, aMA has contributions from (i) photochemical products of atmospheric reactions, (ii) ship effluents in seawater, and (iii) transported coastal and continental emissions from fossil fuel combustion, biogenic, and biomass burning sources. PMA also quickly evolve in the atmosphere due to incorporation and loss of gas phase species. Several studies have focused on characterizing the secondary fraction of organic aerosol particles (SOA) formed through photochemical atmospheric reactions [*O'Dowd et al.*, 2002; *Rinaldi et al.*, 2010; *Facchini et al.*, 2010] (Table 2), but more than 22% of the WSOC fraction of aMA (identified as marine SOA) remains unresolved [*Rinaldi et al.*, 2010]. However, the fact that increases in seawater biological activity or phytoplankton productivity (identified by chlorophyll *a*, chl *a*, concentration) have been linked to increases in the concentration of both PMA (identified as WIOC) and marine-derived SOA (identified as WSOC) submicron particles [*Ceburnis et al.*, 2008; *O'Dowd et al.*, 2004] has confounded attempts to clearly distinguish between primary and secondary organic components in aMA.

Table 2. Selected References Investigating the Organic Composition and Concentration of PMA, gPMA, Secondary, and General aMA Measured in Different Ocean Regions

Reference	Ocean Region[a]	OM Composition	Particle Size (OM, $\mu g\ m^{-3}$)
PMA			
Fu et al. [2013]	Arctic	saccharides	bulk
Leck et al. [2013]	Arctic	heteropolysaccharides	0.035–10 μm
Russell et al. [2010]	Arctic and North Atlantic	polysaccharides	submicron
Hawkins and Russell [2010]	Arctic and Southeast Pacific	polysaccharides, proteins, and phytoplankton fragments	submicron and supermicron
O'Dowd et al. [2004]	Northeast Atlantic (Ireland)	enriched in WIOC with high molecular weight	submicron
Ceburnis et al. [2008]	Northeast Atlantic (Ireland)	WIOC	submicron
Facchini et al. [2008a]	Northeast Atlantic (Ireland)	WIOM	submicron
Bigg and Leck [2008]	Northeast Atlantic (Ireland)	exopolymers	submicron, <200 nm
Ovadnevaite et al. [2011]	Northeast Atlantic (Ireland)	hydrocarbon	submicron
Mochida et al. [2002]	North Pacific	LMW saturated fatty acids	bulk
Sciare et al. [2009]	Austral Ocean	WIOC	bulk
gPMA			
Gao et al. [2012]	Arctic	polysaccharides	bulk
Facchini et al. [2008a]	Northeast Atlantic (Ireland)	WIOM: colloids	submicron
Facchini et al. [2010]	Northeast Atlantic (Ireland)	WIOM: lipopolysaccharides	submicron
Keene et al. [2007]	Northwest Atlantic (Sargasso Sea)	WSOC	submicron and supermicron
Schmitt-Kopplin et al. [2012]	Southeast Atlantic	biomolecules with high aliphaticity	<10 μm
Bates et al. [2012]	Northeast Pacific (Coastal)	polysaccharide-like, alkyl-like, and pattern of CH fragments	submicron
Ault et al. [2013]	Northeast Pacific (Coastal)	aliphatic hydrocarbons	0.15–10 μm
Quinn et al. [2014]	Northeast Pacific (Coastal) and Northwest Atlantic	saccharide-like	submicron
Secondary			
Fu et al. [2013]	Arctic	isoprene product	bulk
O'Dowd et al. [2004]	Northeast Atlantic (Ireland)	enriched in WSOC (partly oxidized species with extended aliphatic moieties)	submicron
Ceburnis et al. [2008]	Northeast Atlantic (Ireland)	WSOC	submicron
Facchini et al. [2008a]	Northeast Atlantic (Ireland)	WSOM	submicron
Facchini et al. [2008b]	Northeast Atlantic	WSOC—dimethyl and diethyl ammonium salts	submicron
Facchini et al. [2010]	Northeast Atlantic (Ireland)	diethyl and dimethyl amine salts	submicron
Rinaldi et al. [2010]	Northeast Atlantic (Ireland)	WSOC: MSA, alkylammonium salts, and dicarboxylic acids	submicron
Meskhidze and Nenes [2006]	Southern Ocean	isoprene product	bulk
Turekian et al. [2003]	Northwest Atlantic (Sargasso Sea)	oxalate	submicron and supermicron
aMA[b]			
Cavalli et al. [2004]	Northeast Atlantic (Ireland)	WIOC; aliphatic and partially oxidized humic-like substances	submicron OC (0.66) and supermicron OC (0.26)
Cavalli et al. [2004]	Northeast Atlantic (Ireland)	WSOC	submicron 0.25
O'Dowd et al. [2004]	Northeast Atlantic (Ireland)	WIOC and WSOC	total OC (0.07, LBA; 0.62, HBA)
Yoon et al. [2007]	Northeast Atlantic (Ireland)		total OC (1.2, spring; 0.1, winter) and submicron OC (0.2, spring; 0.05, winter)
Ovadnevaite et al. [2011]	Northeast Atlantic (Ireland)		submicron (3.8)
Decesari et al. [2011]	Northeast Atlantic	WIOC similar to lipids; WSOC containing fatty acids, alkanoic acids, aliphatic acids, and sulfate esters	submicron
Schmitt-Kopplin et al. [2012]	Southeast Atlantic	biomolecules with high aliphaticity	<10 μm
Crahan et al. [2004]	tropical mid-Pacific	dicarboxylic acids and carbohydrates	<3.5 μm
Kawamura and Gagosian [1987]	North Pacific	oxo-, mono-, and di-carboxylic acids	bulk
Matsumoto and Uematsu [2005]	North Pacific	free amino acids in WSOC	<2.5 μm
Bigg [2007]	Southwest Pacific (Tasmania)	WIOC aggregates and exopolymeric gels	submicron, <200 nm
Shank et al. [2012]	Southeast Pacific		submicron (0.01)
Kuznetsova et al. [2005]	Northwest Mediterranean	proteins, amino acids, and polysaccharides in gels	bulk
Fu et al. [2011]	North Pacific, North Atlantic, Indian, and South China	LMW fatty acids, fatty alcohols, and sterols	bulk

[a]The specific stationary sampling locations are in parentheses.
[b]The OM in the studies in this category were not identified as PMA or secondary and are thus included as general atmospheric marine aerosol particles (aMA).

Contributions from both (ii) seawater pollution and (iii) air pollution from shipping and continental sources are also challenging to characterize since the marine atmosphere mixes rapidly with non-ocean-derived sources, which then also react with solar radiation and trace gases [*Erickson et al*., 1999]. Even in the relatively pristine southeastern Pacific, aMA have been found to have much larger contributions from continental emissions than from PMA OM, the latter of which was frequently below detection [*Hawkins et al*., 2010; *Shank et al*., 2012]. Some measurements that met several criteria for being considered "clean marine" at Mace Head, Ireland (including particle concentrations less than 700 cm^{-3}, black carbon less than 50 ng m^{-3}, and surface wind from the North Atlantic Ocean) still contained carbon that isotopic analysis indicated was 21% from non-ocean sources [*Ceburnis et al*., 2011]. Such results are not surprising given the ubiquity of shipping emissions in many ocean regions [*Coggon et al*., 2012], as well as continental influences. It is exceedingly difficult to reliably exclude shipping and other anthropogenic influences using criteria that consider only wind direction, trajectory classification, black carbon concentration, or particle concentration. Comprehensive criteria are needed to exclude nonmarine sources in order to accurately resolve the PMA portion of aMA.

An alternative approach to study PMA is to create models of the ocean system in which primary marine aerosol particles are produced by artificially generating bubbles in seawater thereby mimicking sea spray production from wave breaking under controlled conditions [*Bates et al*., 2012; *Collins et al*., 2014; *Gao et al*., 2012; *Facchini et al*., 2008a; *Fuentes et al*., 2010; *Hultin et al*., 2010; *Keene et al*., 2007; *King et al*., 2012; *Martensson et al*., 2003; *Sellegri et al*., 2006; *Leck et al*., 2013]. These model-generated primary marine aerosol particles are hereafter referred to as gPMA. The advantage of this approach is that the PMA composition can be studied before it (i) accumulates secondary components or (iii) mixes with shipping or continental emissions. These models have been used to study the organic composition of gPMA for different ocean regions (Table 2), providing insight on the size-dependent composition of gPMA. gPMA from northeastern Atlantic seawater contained WIOC with lipopolysaccharides [*Facchini et al*., 2008a; *Facchini et al*., 2010]. Also, the water-extractable OM fraction of gPMA from Sargasso seawater [*Keene et al*., 2007] and the WIOC fraction of gPMA from northeastern Atlantic seawater [*Facchini et al*., 2008a] increased with decreasing particle size. gPMA from northeastern Pacific seawater were identified to be similar in organic content to polysaccharides and contained a hydrocarbon-like component [*Bates et al*., 2012]. *Gao et al*. [2012] observed enrichment in polysaccharides in gPMA compared to the source seawater from the Arctic. Using seawater from the northeastern Pacific off the coast of Southern California in a wave flume apparatus, *Ault et al*. [2013] observed a change in the structure of hydrocarbon molecules in the gPMA produced from seawater before and after the addition of a culture of bacteria and phytoplankton.

However, none of these studies have measured the extent to which the observed gPMA composition was controlled by the bulk seawater composition or by the potential OM partitioning that occurs during bubble formation, processing, and bursting that produces PMA. A large fraction of dissolved organic carbon (DOC) in the surface ocean is recalcitrant (less biologically available). In addition, the distribution of much of the DOC is controlled by circulation of deep ocean waters [*Hansell*, 2013; *Druffel et al*., 1992]. Still, while seawater is generally known to include saccharides that contribute up to 80% of the high-molecular-weight DOC in seawater [*Aluwihare and Repeta*, 1999; *Aluwihare et al*., 1997; *Benner et al*., 1992], the organic composition of the labile and semilabile (more biologically available) DOC will vary with the phytoplankton populations that are present and their metabolic processes that consume and produce organic components [*Hansell*, 2013]. *Hoffman and Duce* [1976] used the ratio of organic carbon (OC) to Na^+ (OC/Na^+) as a metric for comparing the composition of gPMA and seawater, observing an increase in OC/Na^+ in gPMA from biologically productive seawater. This led them to assert that the chemical form of the organic material could be critical in determining the OC/Na^+ ratio of PMA. Changes in the sea surface biological activity have been shown to alter the surface-active properties of organics and to influence bubble bursting [*Sellegri et al*., 2006]. But are these changes in seawater organic composition reflected in changes in gPMA (and PMA components of aMA) or do other factors have a stronger influence?

In this study, we compare the organic composition of gPMA produced by two different model ocean systems with the organic composition of seawater from three ocean regions that were selected to reflect a range of open-ocean seawater types: (i) Coastal California in the northeastern Pacific, which is influenced by wind-driven, large-scale upwelling leading to productive or eutrophic (nutrient-rich) seawater and high chl *a* concentrations (5 ± 4 μg L^{-1}); (ii) George's Bank in the northwestern Atlantic, which is also influenced by nutrient upwelling and eutrophic seawater with phytoplankton productivity and high chl *a* concentrations

Table 3. The Seawater and Ambient Atmospheric Sampling Conditions During the Collection of the Marine Samples During the Five Projects Given as the Average and Standard Deviation of the Marine Samples

Project (Sample Numbers)	ICEALOT (13)	VOCALS (12)	CalNex (8)	EPEACE (38)	WACS (11)	WACS S1 (3)	WACS S2 (8)
Sampling Period	19 March to 24 April 2008	20 October to 30 November 2008	15 May to 7 June 2010	12–24 July 2011	19–28 August 2012		
Submicron aMA							
OM ($\mu g\ m^{-3}$)	0.44 ± 0.21	0.40 ± 0.17	0.71 ± 0.36	0.62 ± 0.48	1.23 ± 1.29	1.81 ± 1.79	1.14 ± 1.04
O/C	0.96 ± 0.26	0.56 ± 0.11	0.52 ± 0.22	0.61 ± 0.38	0.60 ± 0.34	0.87 ± 0.30	0.50 ± 0.31
Submicron aMA OM Functional Group Composition							
Hydroxyl (%)	58 ± 13	24 ± 7	23 ± 15	41 ± 15	21 ± 16	17 ± 4	22 ± 19
Alkane (%)	21 ± 9	43 ± 7	48 ± 12	43 ± 21	50 ± 20	35 ± 12	53 ± 19
Carbonyl (%)	2 ± 0	NA	NA	NA	NA	NA	NA
Amine (%)	6 ± 3	2 ± 2	3 ± 3	3 ± 6	3 ± 2	3 ± 3	3 ± 3
Acid (%)	14 ± 8	30 ± 5	26 ± 11	13 ± 15	26 ± 21	48 ± 8	23 ± 19
Seawater Characteristics							
SST (°C)	6 ± 3	19 ± 1	14 ± 1	14 ± 1	27 ± 4	19 ± 3	28 ± 1
Chl *a* ($\mu g\ L^{-1}$)	NA	NA	5.0 ± 4.0	0.4 ± 0.6	0.8 ± 2.3	3.6 ± 2.7	0.1 ± 0.1
Salinity	34.7 ± 0.5	35.0 ± 0.1	33.2 ± 0.2	33.5 ± 0.2	35.4 ± 1.5	32.4 ± 0.4	35.9 ± 0.4
Atmospheric Conditions							
Temperature (°C)	1 ± 7	13 ± 1	13 ± 1	14 ± 1	26 ± 4	19 ± 2	27 ± 1
Wind speed ($m\ s^{-1}$)	11 ± 4	7 ± 2	5 ± 2	13 ± 5	4 ± 2	2 ± 1	5 ± 2
Radon ($mBq\ m^{-3}$)	315 ± 108	106 ± 75	811 ± 664	NA	301 ± 365	725 ± 88	233 ± 322
Black carbon ($ng\ m^{-3}$)	<60[a]	10[b]	NA	<2[c]	NA	NA	NA

[a]Campaign average estimated from *Frossard et al.* [2011].
[b]Campaign average from *Shank et al.* [2012].
[c]From *Wonaschutz et al.* [2013]. Campaign split into two regimes with different average black carbon concentrations (1.03 ± 1.06 $ng\ m^{-3}$ and 1.8 ± 1.01 $ng\ m^{-3}$).

(7 ± 2 $\mu g\ L^{-1}$); and (iii) the Sargasso Sea in the subtropical western Atlantic, which is oligotrophic and nutrient limited, reflected in low phytoplankton productivity and low chl *a* concentrations (0.03 ± 0.05 $\mu g\ L^{-1}$) (Table 1). In order to provide as complete as possible characterizations of the organic fraction of aMA, here we use Fourier transform infrared (FTIR) spectroscopy because it provides information about the functional group composition that is characteristic of aMA [*Russell et al.*, 2010] and represents the marine organic fraction more completely than is possible with techniques that measure nonrefractory mass (vaporizable at 650°C) [*Frossard et al.*, 2014]. The three questions that are addressed in this work are the following: (i) what is the organic functional group composition of ocean-derived aMA? (ii) how much of aMA composition can be explained by generating primary marine aerosol (gPMA) from bubbled seawater? and (iii) what are the differences between the organic compositions of gPMA and seawater?

2. Methods

The organic functional group composition of submicron aMA was measured during five shipboard campaigns (Table 3). During two of the cruises, gPMA and seawater OM compositions were also measured. The tracks for each campaign are overlaid in Figure 1. In this study we use aMA measurements from all five cruises to provide additional context for the two campaigns during which gPMA and seawater OM were also characterized, in regions representing broad ranges in seawater productivity (and chl *a* concentrations), sea surface temperature, and other air-sea conditions.

2.1. Shipboard Campaigns That Sampled Open-Ocean aMA

aMA were characterized in the MBL during (i) the International Chemistry Experiment in the Arctic Lower Troposphere (ICEALOT) project in March and April 2008 onboard the R/V *Knorr* in the North Atlantic and Arctic Oceans; (ii) the VAMOS Ocean-Cloud-Atmosphere-Land Study Regional Experiment (VOCALS) in October 2008 onboard the R/V *Ronald H. Brown* in the southeastern Pacific; (iii) the California research at the Nexus of Air Quality and Climate Change study (CalNex) in May and June 2010 onboard the R/V *Atlantis*, which traveled from San Diego to Sacramento, California; (iv) the Eastern Pacific Emitted Aerosol Cloud Experiment (EPEACE) in July 2011 onboard the R/V *Point Sur* off the coast of Moss Landing, California; and (v) the Western Atlantic Climate Study (WACS) in August 2012 onboard the R/V *Ronald H. Brown* that traveled from

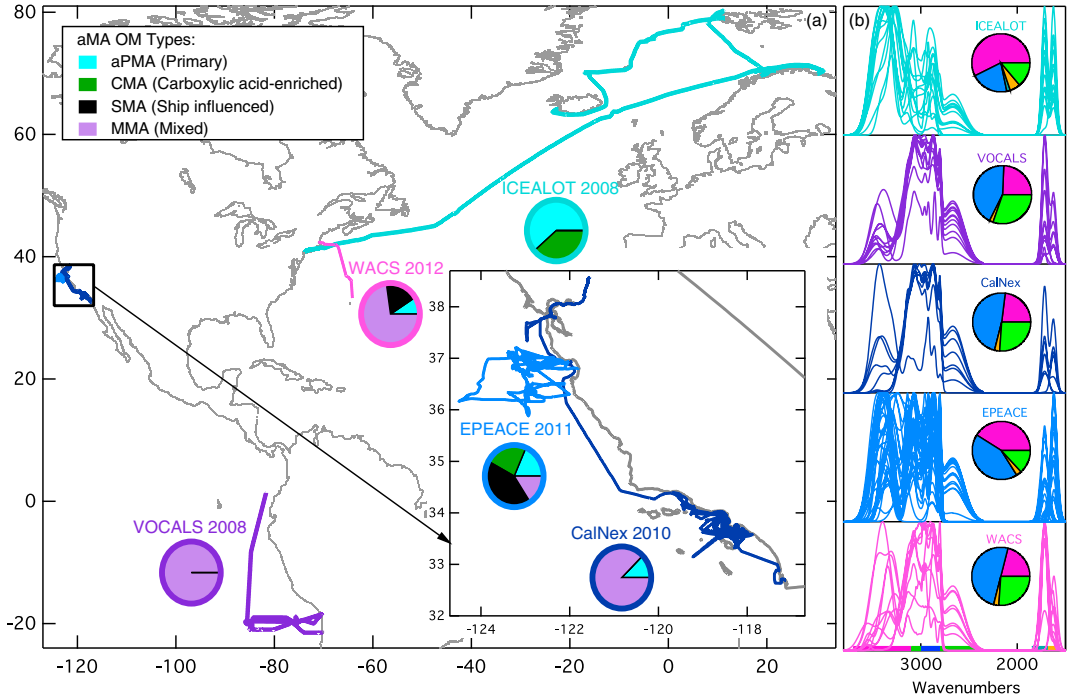

Figure 1. (a) Map of the cruise tracks for ICEALOT, VOCALS, CalNex, EPEACE, and WACS. The pie charts at each location represent the fraction of samples associated with each aMA OM type shown in the legend. (b) Comparison of the normalized organic FTIR spectra of the marine samples from the five projects. The pie charts represent the corresponding mean organic functional group compositions with hydroxyl (pink), alkane (blue), carboxylic acid (green), carbonyl (teal), and amine (orange).

Boston, Massachusetts, sampling first at George's Bank (Station 1) and then in the Sargasso Sea (Station 2) before continuing on to St. George's, Bermuda. During ICEALOT, VOCALS, CalNex, and WACS, aMA were sampled through a humidity- and temperature-controlled isokinetic, wind-pointing inlet, similar to that described by *Bates et al*. [2002], at ~18 m above sea level; EPEACE used a simple vertical tube inlet with a lower flow rate for submicron particles [*Russell et al*., 2013; *Wonaschutz et al*., 2013]. Additional sampling conditions during each campaign are given in Table 3, including average sea surface temperature (SST), seawater chl *a* concentrations, salinity, air temperature, wind speed, and atmospheric radon concentrations, which is a decay product of crustal material and can be used as a measure of the continental influence of the sampled air masses.

2.2. Model Ocean Systems Used for Producing gPMA

During CalNex and WACS, two marine aerosol generators were used to model bubble bursting at the ocean surface: the Sea Sweep and the Bubbler. gPMA were generated in the biologically productive seawater at WACS Station 1 and CalNex and the nonproductive, oligotrophic seawater at WACS Station 2 [*Quinn et al*., 2014] in order to determine the influence of the seawater productivity on the OM composition of the gPMA.

The Sea Sweep generator consists of a stainless steel frame attached to a small raft that was deployed off the port bow of the R/V *Atlantis* and R/V *Ronald H. Brown* [*Bates et al*., 2012]. Stainless steel frits were positioned at 0.75 m below the sea surface. While on station and steaming slowly forward to maintain continuous renewal of sea surface water, zero air (charcoal and HEPA, high efficiency particulate air, filtered [*Bates et al*., 2012]) was pumped through the frits to create bubbles that burst at the seawater surface. The resulting gPMA in sample air were directly transported to the instruments for analysis. A curtain of particle-free air prevented ambient air from mixing with the bubbling seawater.

The Bubbler models the ocean using a 20 cm diameter 40 L Pyrex cylinder into the base of which fresh seawater was pumped at 4 L min^{-1} from the bow of the ship at 5 m below the sea surface [*Keene et al*., 2007]. Seawater drained to waste evenly over the top annular rim, continuously replacing surface seawater and

minimizing the formation of standing bubble rafts [*Long et al*., 2014]. Bubbles were produced at a mean depth of 84 cm below the model sea surface using zero air (see section 7.4 in the supporting information for description) pumped through fine or coarse-sintered glass frits at varying flow rates (1.5 to 6 L min^{-1}). The Bubbler was also equipped with glass tubes that could be configured to generate gPMA by impinging jets of fresh seawater onto the model sea surface. Purified zero air hydrated to 80 (±2)% relative humidity transferred gPMA under laminar flow to instruments for characterization of number size distributions and size-resolved and bulk chemical composition. The number size distributions and average compositions of gPMA from the different production configurations are compared in Figure S1 in the supporting information.

2.3. Aerosol and Related Measurements

2.3.1. Chemical Analysis of Particles Collected on Filters

Submicron aMA were dried by a diffusion dryer filled with silica gel on EPEACE and WACS and by a temperature- and humidity-controlled inlet on ICEALOT, VOCALS, and CalNex. Submicron Sea Sweep gPMA were dried by a temperature- and humidity-controlled inlet during CalNex. The Bubbler gPMA from CalNex were not size selected or dried before collection. Submicron Sea Sweep and Bubbler gPMA were dried by a diffusion dryer filled with silica gel during WACS. aMA and gPMA were collected on 37 mm Teflon filters (Pall Inc., 1 μm pore size) at a flow rate of 8 L min^{-1} for 1 to 20 h. The filters were frozen and transported to the laboratory for analysis by FTIR spectroscopy (Bruker Tensor 27 spectrometer with deuterated triglycine sulfate, DTGS, detector) to measure the infrared transmission using 2 cm^{-1} resolution [*Takahama et al*., 2013; *Frossard et al*., 2011; *Hawkins et al*., 2010]. The gPMA filter samples were dehydrated prior to analysis, as described by *Frossard and Russell* [2012], which consisted of freezing and gently heating the samples. During WACS and EPEACE, FTIR scans were carried out onboard the research vessel prior to freezing to evaluate possible effects of transport and storage; no artifacts from transport and storage were identified in either the OM composition or concentration.

During CalNex and WACS, unfiltered seawater from the 5 m below sea surface bow seawater line was collected from the sampling regions in sterile glass mason jars, atomized (TSI constant output atomizer 3076), and then collected on Teflon filters without size segregation. The atomized seawater samples were dehydrated using the procedure outlined by *Frossard and Russell* [2012] prior to analysis to remove interference of sea-salt hydrate bound water with the organic signal in the FTIR spectra.

The FTIR spectrum from each filter was analyzed using an automated algorithm [*Maria et al*., 2002; *Russell et al*., 2009; *Takahama et al*., 2013], briefly described here. First, the spectrum of each filter prior to sampling was subtracted from the spectrum after sampling, in order to remove any contribution from scattering and absorption of the filter, following the procedure described by *Maria et al*. [2003]. Then the remaining spectrum was baselined from 4000 to 2000 cm^{-1} using a third-order polynomial and from 2000 to 1400 cm^{-1} using a line, with details provided by *Takahama et al*. [2013]. The absorption shown by the baselined spectrum was apportioned by fitting parameterized Gaussian distributions to given regions of the spectrum [*Takahama et al*., 2013]. A measured spectrum from NH_4^+ was scaled and subtracted from the sample spectrum before any other peak quantification [*Takahama et al*., 2013]. The absorptivity and molar mass were used to convert peak area to mass for each organic functional group including: organic hydroxyl (C-O-H), alkane (C-C-H), amine (C-N-H), carboxylic acid (COOH), and nonacid carbonyl (C = O). The micromoles of alkene (C = C-H) and aromatic functional groups, calculated from the absorptivities, were below the detection limit in all of the samples and are excluded from this discussion. The detection limits of each functional group were determined using this technique and are listed by *Russell et al*. [2009] (see Table S4 in the supporting information). The total OM analyzed in each sample was calculated as the sum of the concentrations of the organic functional groups. The OM measured by this technique, including the FTIR analysis and the integration algorithm, has an uncertainty of 20% [*Maria et al*., 2002; *Russell et al*., 2013; *Takahama et al*., 2013], indicating that the fitting and calibration of each functional group results in 20% uncertainty in its mass. This 20% could consist of functional groups that were below detection by FTIR spectroscopy in the gPMA and atomized seawater samples but have been previously observed in marine regions, such as amide and carboxylic acid groups. The molar ratio of oxygen to carbon (O/C) was calculated by summing the moles of oxygen in oxygen-containing functional groups (hydroxyl, carboxylic acid, and nonacid carbonyl) and dividing by the total moles of carbon in all observed functional groups for each sample

[*Russell et al.*, 2009]. Converting the total moles of carbon to mass gives the total organ carbon (OC) mass of the samples. After nondestructive FTIR analysis, X-ray fluorescence (XRF) (Chester LabNet, Tigard, Oregon) was used to quantify the elemental masses for elements Na^+ and heavier on the filters [*Maria et al.*, 2003] sampled during ICEALOT, VOCALS, and EPEACE.

During ICEALOT, VOCALS, CalNex, and WACS, submicron aMA were collected, and during CalNex and WACS, submicron Sea Sweep gPMA were collected with a Berner-type multijet cascade impactor. Particles were impacted on Millipore Fluoropore filters, and the substrates from these filters were extracted and analyzed using ion chromatography to quantify inorganic ions including Na^+, Cl^-, SO_4^{2-}, NO_3^-, and NH_4^+ [*Quinn et al.*, 1998].

Sea-salt concentrations were calculated using ion chromatography measurements for ICEALOT, VOCALS, CalNex, and WACS and XRF measurements for EPEACE. For the gPMA, sea-salt concentration equals 3.26 times the Na^+ mass, based on the calculation by the ratio of $(Na^+ + Mg^{2+} + Ca^{2+} + K^+ + Cl^- + SO_4^{2-} + HCO_3^-)/Na^+$ in seawater [*Holland*, 1978]. Atmospheric ambient sea-salt concentrations were calculated using measured Cl^- and 1.47*Na^+ concentrations to account for the possible depletion of Cl^- in the atmosphere, where 1.47 is the ratio of $(Na^+ + Mg^{2+} + Ca^{2+} + K^+ + SO_4^{2-} + HCO_3^-)/Na^+$ in seawater [*Holland*, 1978]. This sea-salt calculation represents an upper limit for sea-salt mass because the HCO_3^- would have been titrated before Cl^- was depleted significantly via acid displacement reactions. HCO_3^- is 0.3% of the total mass of sea salt. Excluding HCO_3^- from the ratio, as a lower limit, the ratio of $(Na^+ + Mg^{2+} + Ca^{2+} + K^+ + SO_4^{2-} + HCO_3^-)/Na^+$ is 1.45, instead of 1.47, making the salt mass calculated $<2\%$ lower than calculated here.

2.3.2. Single-Particle Measurements

During CalNex and WACS, aMA (0.39–2.6 μm) and gPMA (0.65–3.1 μm) were collected on silicon nitride windows (Si_3N_4, Silson Ltd, Northampton, UK) using a Streaker impactor (PIXE International Corp., Tallahassee, FL). The windows were frozen after collection to prevent evaporation. Particles were collected for 30 to 90 min, depending on the particle number concentrations. The windows were analyzed at the Advanced Light Source at Lawrence Berkeley National Laboratory using scanning transmission X-ray microscopy with near edge X-ray absorption fine structure (STXM-NEXAFS) to determine the morphology and organic composition of the single particles [*Hawkins and Russell*, 2010; *Takahama et al.*, 2007, 2010].

2.3.3. Other Measurements

Meteorological parameters that were measured include temperature, wind speed, wind direction, and solar radiation. Measured seawater parameters include salinity, sea surface temperature (SST), and fluorescence (relative chl *a* concentrations). The continuous fluorescence signal for each cruise was calibrated for chl *a* concentration using discrete samples of seawater collected during the cruise and a commercially available chl *a* standard [*Bates et al.*, 2012].

3. Results

This study focuses on atmospheric "marine" aerosol particles (aMA), where we define marine in the sense of noncontinental to mean OM types that meet the three criteria discussed in section 3.1. In this sense, aMA includes both natural emissions from the pristine open-ocean as well as man-made emissions from ocean-based activities, such as shipping, and some coastal (or other continental) anthropogenic emissions transported to open-ocean regions often after some amount of dilution. This section summarizes and classifies the measured composition of the samples that meet this definition of aMA and compares the composition of gPMA and seawater OM.

3.1. Classification of aMA

Three criteria were used to distinguish aMA from nonmarine aerosol particles. First, aMA samples collected within 1 km of a port or land were excluded. Second, sampling was controlled using automated valves to suspend sampling during periods when particle concentrations (generally greater than 1000 cm^{-3}) indicated the presence of ship exhaust. This conditioned sampling excluded sampling of direct emissions of nearby ships and of the research vessel itself. Third, only samples with air mass back trajectories, calculated using the isentropic Hybrid Single-Particle Lagrangian Integrated Trajectory (HYSPLIT) model [*Draxler and Rolph*, 2003], of predominantly marine origin (3 day back trajectories that originated from over the ocean and spent more than 75% of the sampling time over the ocean) were considered to be marine for this analysis.

Additional project-specific criteria used in the aMA sample selection and description of the HYSPLIT back trajectories are included in section 7.1 in the supporting information. All of the aMA samples discussed here met all three of these criteria.

3.2. Comparison of aMA OM From Five Marine Regions

The mean organic compositions of submicron aMA measured by FTIR spectroscopy during five research cruises are shown in Figure 1b and summarized in Table 3. Submicron aMA OM was sampled during ICEALOT in the North Atlantic and Arctic Oceans (Figure 1a). The average SST during ICEALOT was 6 (±3)°C, which is lower than CalNex, EPEACE, VOCALS, or WACS, and ICEALOT aMA OM had the largest fraction of hydroxyl functional groups (58%) compared to the other studies (Table 3). During VOCALS, aMA were collected in the southeastern Pacific (Figure 1a). The average submicron aMA OM was 0.40 (±0.17) $\mu g\,m^{-3}$, and the average OM composition is shown in Table 3.

During CalNex, the submicron aMA OM concentrations ranged from 0.13 to 1.45 $\mu g\,m^{-3}$ and averaged 0.71 (±0.36) $\mu g\,m^{-3}$ (Table 3), which is higher than OM concentrations sampled in other regions (Table 3). The CalNex samples have higher alkane and carboxylic acid functional group fractions than previous measurements of OM identified as PMA (10–15% and less than 10%, respectively) [*Russell et al*., 2010]. The average ratio of O/C for the submicron aMA OM during CalNex was 0.52, indicating that the marine OM was also highly oxygenated.

During EPEACE, the concentration of submicron aMA OM ranged from 0.06 to 1.09 $\mu g\,m^{-3}$ with an average of 0.62 (±0.48) $\mu g\,m^{-3}$ (Table 3). The mean OM composition is given in Table 3, but the composition varied substantially in the FTIR spectra of the EPEACE samples (Figure 1b). The fraction of carboxylic acid functional groups in the aMA OM was similar to ICEALOT and lower than that of the aMA OM from other regions. The wind speed during sampling ranged from 5 to 24 $m\,s^{-1}$ with an average of 13 (±5) $m\,s^{-1}$, which is sufficiently high for wave breaking and active production of PMA. The chl *a* concentration was variable while the seawater salinity, air temperature, and SST were relatively constant (Table 3).

During the WACS cruise (Figure 1a), submicron aMA OM was 1.23 (±1.29) $\mu g\,m^{-3}$ with the mean composition given in Table 3. Submicron aMA OM was sampled during two periods with distinct atmospheric and seawater properties (Table 3). The more biologically productive seawater of Station 1 had higher average chl *a* concentrations ($3.6 \pm 2.7\,\mu g\,L^{-1}$), which were variable but stayed well above oligotrophic seawater concentrations ($0.1\,\mu g\,L^{-1}$). The air temperature, SST, and salinity were lower than Station 2 (Table 3). The average OM was higher at Station 1 ($1.81 \pm 1.79\,\mu g\,m^{-3}$), and the average composition was 17 (±4)% hydroxyl, 35 (±12)% alkane, 3 (±3)% amine, and 48 (±8)% carboxylic acid functional groups. The oligotrophic, nonproductive seawater at Station 2 showed little variability in the low average chl *a* concentration of 0.06 (±0.08) $\mu g\,m^{-3}$. The average OM was 1.14 (±1.04) $\mu g\,m^{-3}$ with a mean composition of 22 (±19)% hydroxyl, 53 (±19)% alkane, 3 (±3)% amine, and 23 (±19)% carboxylic acid functional groups.

3.3. Source Identification of Atmospheric Marine Aerosol Particles (aMA) OM

Ward cluster analysis [*Ward*, 1963] was used to classify the individual FTIR spectra of submicron aMA OM collected during all of the projects. Results yielded four clusters of samples (Figure 2), each of which differs from the others in that the cosine similarities of the characteristic spectra to each other are lower (by 0.1) than the cosine similarity of the spectra within each cluster (additional details in section 7.2 in the supporting information). Based on the atmospheric and seawater conditions, locations during sampling, and spectral features, these aMA OM types were characterized as (i) atmospheric primary marine aerosol particles (aPMA), (ii) carboxylic acid-enriched PMA (CMA), (iii) shipping-influenced marine aerosol particles (SMA), and (iv) mixed marine aerosol particles (MMA). Of these four aMA types, only aPMA and CMA are considered "clean" in the sense of being derived from the natural ocean (with CMA also including atmospheric contributions that may be from ocean-derived biogenic volatile organic compounds, as discussed below). While all four aMA OM types are marine, based on the selection criteria in section 3.1, SMA and MMA have compositions and OM spectral signatures indicative of anthropogenic sources, as described in later sections. Since individual atmospheric samples generally include contributions from more than one source, this classification categorizes samples based on the source that contributes the majority of the OM and denotes as MMA samples for which multiple OM types each contributed, as summarized in Table 1. CMA, SMA, and MMA OM types all have some aPMA contribution, and in addition, they contain OM contributions from other sources.

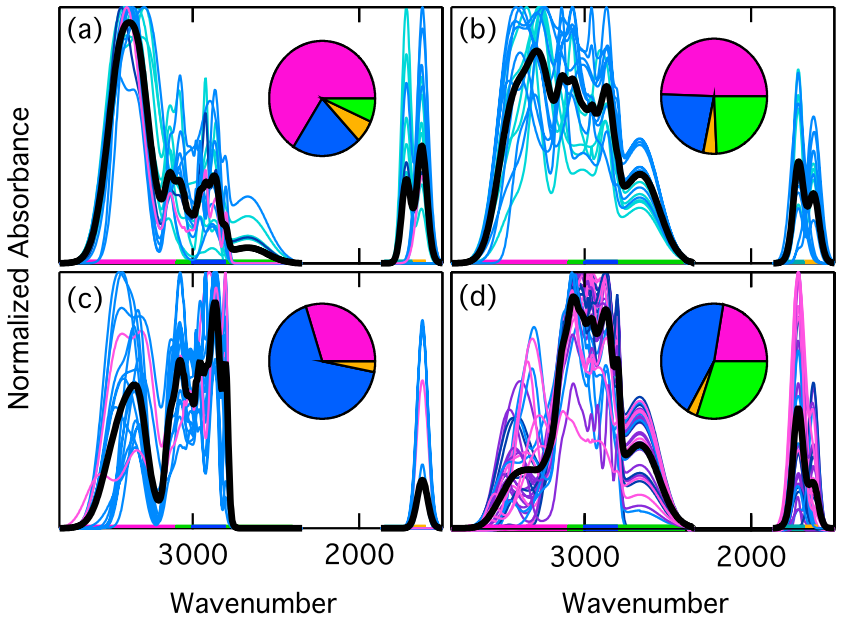

Figure 2. Normalized FTIR spectra of submicron aMA separated into four marine OM types: (a) aPMA, (b) CMA, (c) SMA, and (d) MMA. The thick black lines are the average spectra of each OM type. Individual spectra are colored by project including ICEALOT (teal), VOCALS (purple), CalNex (dark blue), EPEACE (light blue), and WACS (pink). The pies represent the average functional group composition of each OM type with hydroxyl (pink), alkane (blue), carboxylic COH (green), and amine (orange) functional groups.

The clustering identifies either the lack of substantial contributions (<30%) from anything but ocean-derived biogenic sources (aPMA), or the mixture of aPMA sources with carboxylic acid (CMA), shipping (SMA), or multiple other mixed sources (MMA). The fraction of OM associated with these source types was tested by creating artificial mixtures with varying quantities of the aMA OM types and reexecuting the clustering algorithm. The four aMA OM types and their production processes are shown in Figure 3, in addition to their relation to gPMA. A description of each OM type and the basis for each classification are given in the following paragraphs.

The atmospheric primary marine aerosol particles (aPMA) have an average OM of 0.45 $\mu g\,m^{-3}$ and a functional group composition of 65 (±12)% hydroxyl, 21 (±9)% alkane, 6 (±6)% amine, and 7 (±8)% carboxylic acid (Figure 2a), where the variability is indicated as 1 standard deviation (Table 4). This OM type was present during 23% (17 samples) of the total sampling time included in this study and was observed during ICEALOT, EPEACE, CalNex, and WACS (Figure 1a). The aPMA was more frequently identified during high wind speeds, typically 5 to 24 $m\,s^{-1}$ with an average of 13 $m\,s^{-1}$. All but two of the samples had average wind speeds greater than 7.3 $m\,s^{-1}$, and all of the samples contained periods with wind speeds greater than 10 $m\,s^{-1}$, which allowed for sufficient wave breaking (wind speeds greater than 8 $m\,s^{-1}$) and bubble bursting [*Gantt et al.*, 2011]. The wind speed of the aPMA samples correlates with submicron Na^+ concentrations ($r = 0.70$), consistent with a wind-driven source such as aPMA production. This is also consistent with previous studies that have shown a correlation between wind speed and PMA production in the open ocean [*Nilsson et al.*, 2001]. Eight of the 17 aPMA samples were collected at high latitude during ICEALOT at relatively high wind speeds, low temperatures, and low solar radiation, supporting the primary nature of this OM.

The average Na^+/Cl^- ratio for samples in the aPMA OM type is 0.74 (±0.15), which is higher than the Na^+/Cl^- mass ratio of seawater (0.56) [*Lewis and Schwartz*, 2004], likely due to Cl^- depletion by acid displacement [*Buseck and Posfai*, 1999; *Keene et al.*, 1998; *Lewis and Schwartz*, 2004; *Pszenny et al.*, 1993]. The aPMA Na^+/Cl^- ratio is within 25% of the Na^+/Cl^- ratio of seawater, and the lower values fall close to the ratio for seawater, consistent with this OM being classified as largely primary from a seawater source. The similarity of the Na^+/Cl^- ratio in the aPMA to that of seawater indicates that little Cl^- has been depleted (irreversibly) since its emission into the atmosphere.

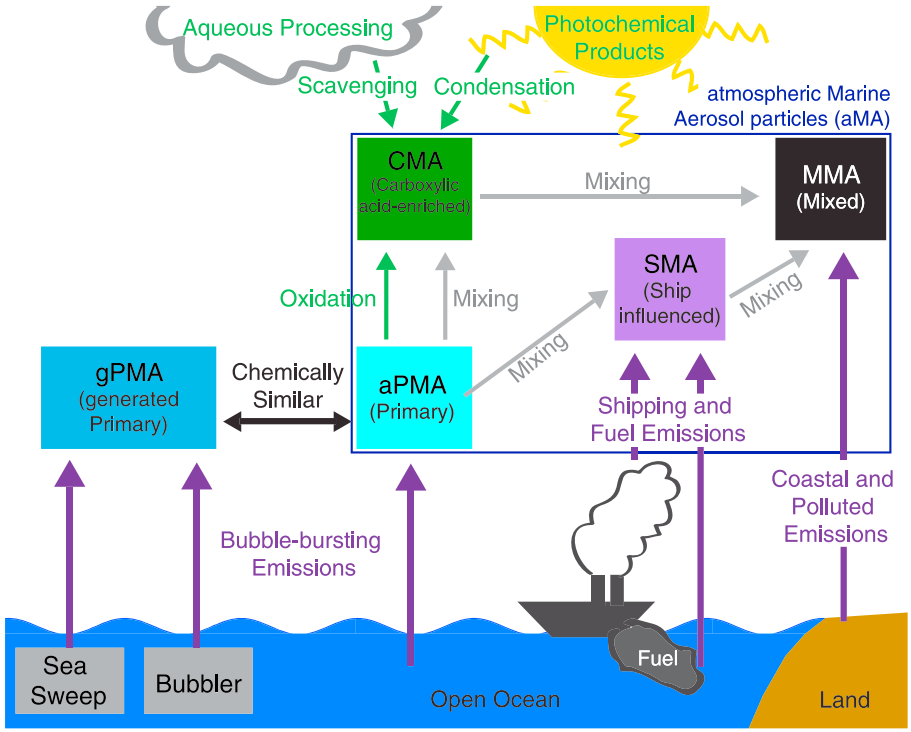

Figure 3. Diagram illustrating the categories of marine aerosol types used in this paper: generated marine aerosol particles (gPMA), atmospheric primary marine aerosol particles (aPMA), aPMA with secondary carboxylic acid marine aerosol particles (CMA), shipping-influenced marine aerosol particles (SMA), and mixed marine aerosol particles (MMA). aPMA, CMA, SMA, and MMA are the four aMA OM types. These mixing arrows show the contribution of aPMA to the other three OM types. Additionally, aPMA may contain up to 30% of other sources.

The second clean marine OM type was identified as carboxylic acid-enriched primary marine aerosol particles (CMA), namely, marine OM that includes more than 10% carboxylic acid functional groups by mass. CMA has an average composition of 49 (±6)% hydroxyl, 24 (±7)% alkane, 4 (±4)% amine, and 22 (±6)% carboxylic acid functional groups (Figure 2b), and the ranges represent the variability as 1 standard deviation (Table 4). This OM type was observed during 14% of the total sampling time (14 of the samples) in this study and only during ICEALOT and EPEACE (Figure 1a), both of which had frequent boundary layer clouds. The sampling conditions were similar to the aPMA OM type conditions but had slightly lower average wind speeds (11 m s^{-1}), still

Table 4. Mean Molar Ratios, Mass Ratios, and Functional Group Mass Compositions of aMA OM, gPMA OM, and Seawater OM

	Molar Ratios		Mass Ratio	Functional Group Mass Composition			
	O/C	C/N[a]	OC/Na^+	Hydroxyl	Alkane	Amine	Carboxylic Acid
aMA OM Types							
aPMA	1.03	9.8	0.45	65 ± 12	21 ± 9	6 ± 6	7 ± 8
CMA	0.93	17.4	1.07	49 ± 6	24 ± 7	4 ± 4	22 ± 6
SMA	0.25	24.9	7.3	31 ± 5	66 ± 6	3 ± 6	0
MMA	0.54	68.1	5.9	23 ± 7	45 ± 13	2 ± 2	30 ± 11
gPMA OM[b,c]	0.68	6.9	0.27 ± 0.15	55 ± 14	32 ± 14	13 ± 3	0
Productive	0.50	7.4	0.30 ± 0.15	45 ± 10	42 ± 9	13 ± 4	0
Nonproductive	0.90	6.9	0.18 ± 0.11	65 ± 10	22 ± 10	12 ± 3	0
Seawater OM[c]	1.0	8.0	NA	71 ± 4	17 ± 5	11 ± 6	0

[a]Typical Redfield ratio for seawater C/N is 6.6 [*Redfield*, 1934]; aPMA, CMA, SMA, and MMA averages only include samples that contain nonzero moles of N.
[b]Includes all Sea Sweep and Bubbler samples.
[c]WACS only.

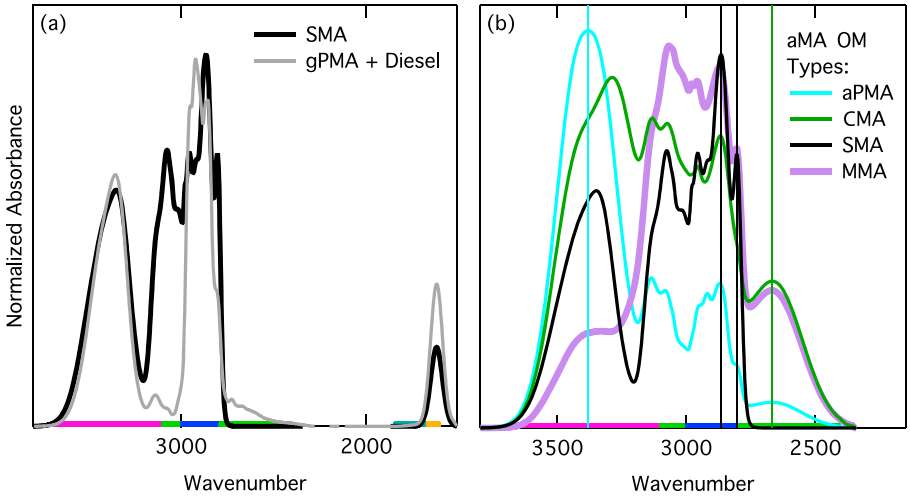

Figure 4. Normalized FTIR spectra of (a) SMA and gPMA with ship diesel and (b) the four aMA OM types. The spectral similarities are shown with vertical lines in Figure 4b at the aPMA max hydroxyl group peak location (3380 cm^{-1}), the SMA alkane group signatures (2865 and 2804 cm^{-1}), and the CMA carboxylic acid group peak (2668 cm^{-1}).

sufficient for local wave breaking and hence for PMA production. The Na^+/Cl^- ratio (0.80 ± 0.20) is similar to that of the aPMA, consistent with aerosol particles that have not been depleted in Cl^-.

The third OM type was identified as shipping-influenced marine aerosol particles (SMA) OM and contains 31 (±5)% hydroxyl, 66 (±6)% alkane, and 3 (±6)% amine functional groups (Figure 2c and Table 4). SMA was observed during 11% of the total sampling time (18 samples), mainly as part of EPEACE and WACS (Figure 1a). During WACS, one of the two SMA samples was collected near (approximately 100 km) the port of Bermuda. The spectra of the SMA OM type have features indicative of a long-chain alkane-type species with absorption peaks at 2981, 2956, 2923, 2865, 2804 cm^{-1}. The peaks at 2923 and 2865 cm^{-1} represent repeating unsaturated CH_2 groups [*Pavia et al*., 2001]. These signatures have been observed in FTIR spectra of ship diesel and other fuels prior to combustion [*Guzman-Morales et al*., 2013] and direct ship stack emissions [*Wonaschutz et al*., 2013]. The similarity between the SMA spectrum and a spectrum of gPMA added to a ship diesel spectrum illustrates the likely contribution of alkane-rich fuel and shipping emissions to the SMA OM (Figure 4a). The SMA OM has the highest average fraction of alkane functional groups (66% ± 6%) compared to the other marine OM types (Table 4) and has a significantly larger alkane functional group fraction than aPMA (21 ± 9%) and CMA (24 ± 7%). SMA also contains no carboxylic acid functional groups (Figure 2), which indicates that these particles did not have detectable contributions from aqueous or photochemical processing. Also, the fuel signatures could originate from incorporation of ship effluent in surface seawater, which is then transferred to the aerosol particles via PMA production, as discussed in section 4.2.3. The average fractions of hydroxyl and amine functional groups likely indicate a contribution from organic aPMA. The corresponding wind speeds during these sampling times had an average of 11 m s^{-1}, which is fast enough to produce PMA from ambient bubble bursting.

The last type of aMA OM was identified as mixed marine aerosol particles (MMA) due to the evidence for contributions of aPMA, CMA, and SMA, as well as continental (anthropogenic) sources, in varying amounts (Figure 4b). MMA composition was 23 (±7)% hydroxyl, 45 (±13)% alkane, 2 (±2)% amine, and 30 (±11)% carboxylic acid functional groups, with an average OM of 0.53 μg m^{-3} (Figure 2d and Table 4). Thirty-three of the aMA samples are MMA, which corresponds to 51% of the total sampling time in this study. MMA was observed during VOCALS, CalNex, EPEACE, and WACS (Figure 1a). The composition and spectrum of this OM type have features of the other three aMA OM groups, including (i) a similar average hydroxyl group peak location (3380 cm^{-1}) to aPMA (3377 cm^{-1}) within the method uncertainty of ±6 cm^{-1} for hydroxyl group peak location (measured with replicates of atomized ribose standards [*Takahama et al*., 2013]), (ii) alkane functional group double peaks at 2957 and 2806 cm^{-1} similar to SMA (2956 and 2804 cm^{-1}) within the method uncertainty of ±3 cm^{-1} for alkane group peak location, and (iii) a carboxylic acid functional group fraction (30 ± 11%) within the measured variability of the carboxylic acid functional group fraction of CMA

(22 ± 6%) (Figure 4b). These samples were collected during the lowest average wind speed periods (7 m s^{-1}), suggesting that there was little local production that contributed to aPMA from bubble bursting (consistent with the lower sea-salt concentration of less than 0.1 μg m^{-3} compared to aPMA which had more than 1 μg m^{-3}). The high Na^+/Cl^- ratio (2.6 ± 1.3), in the absence of crustal sources of Na^+, is likely the result of Cl^- depletion by acid substitution in seawater-derived NaCl. The high level of depletion of Cl^- in the MMA (relative to aPMA or CMA) is consistent with atmospheric reactions in particles that have more inorganic acid present (relative to aPMA or CMA), which is more likely associated with anthropogenic sources of NO_3^- (such as NO_x from combustion) associated with either shipping or other continental fossil fuel burning sources (consistent with the presence of multiple source types in MMA). The average spectrum of MMA OM is similar to spectra observed from continental and anthropogenic sources, such as the oxidized fossil fuel combustion source identified by *Guzman-Morales et al.* [2013] using positive matrix factorization (PMF) during CalNex. The 7 CalNex samples in this OM type all have characteristic absorption similar to that of oxidized combustion sources, indicating that one contribution to MMA in CalNex is oxidized fossil fuel combustion emissions. In addition, these CalNex samples were sampled close to the California coast, consistent with the possible contribution of continental sources.

The number of samples of each aMA OM type for the individual projects is shown in Figure 1a. During CalNex, of the 8 aMA samples, only 1 was determined to be aPMA, while the other 7 were MMA, indicating that during the CalNex sampling, close to the coast of California, there was very limited time in which polluted marine (continental or ship) emissions did not impact the OM composition. The EPEACE aMA OM included 7, 9, and 6 of the samples in the aPMA, CMA, and MMA OM types, respectively, as well as 16 samples identified as SMA. This large number of SMA samples is consistent with the large contribution of shipping emissions to the aMA OM in the northeastern Pacific [*Coggon et al.*, 2012]. During WACS, 1 of the 11 samples was determined to be the aPMA OM type, while 2 were SMA, and 8 were MMA OM. All of the 12 aMA samples from VOCALS were determined to be MMA OM, with no clean marine OM observed during this sampling period. While some primary marine aerosol was included in the samples collected during VOCALS, the long sampling time required for the low OM concentrations along with the offshore flow and low local wind speed meant that the PMA was always mixed with signatures from shipping, anthropogenic activities, or carboxylic-enriched aerosol. This observation is consistent with the identification of "polluted marine" particles observed by *Hawkins et al.* [2010]. In contrast, the ICEALOT sampling region contained only samples identified as clean aMA OM with 8 aPMA and 5 CMA samples.

3.4. Organic Composition of gPMA

Sea Sweep and Bubbler gPMA generated during CalNex and WACS were similar in composition with large fractions of hydroxyl, some alkane, and small fractions of amine functional groups, with an overall average composition of 55 (±14)% hydroxyl, 32 (±14)% alkane, and 13 (±3)% amine functional groups (where the ranges represent the observed variability as 1 standard deviation as shown in Table 4). No detectable carboxylic acid functional group mass was observed in any of the gPMA samples.

The Sea Sweep flow rates were not comparable to the Bubbler, so the comparison between the two model ocean systems is based on the relative fractions of organic components in the gPMA rather than the absolute concentrations. During WACS, the Sea Sweep gPMA showed a higher average OC/Na^+ ratio produced at Station 1 (productive) than at Station 2 (nonproductive) with 0.28 (±0.13) and 0.17 (±0.13), respectively, but the difference between the two stations (0.09) is smaller than the variability within each station (0.13), as reported by *Quinn et al.* [2014]. The Bubbler used a controlled airflow rate that was varied from 1.5 to 6 L min^{-1} (see section 7.4 in the supporting information). At the same flow rate of 4 L min^{-1}, the Bubbler gPMA had an OC/Na^+ of 0.51 (±0.06) in productive (Station 1) seawater and 0.19 (±0.06) in oligotrophic (Station 2) seawater. While the station-to-station difference of 0.32 for the Bubbler gPMA samples is larger than for the Sea Sweep, the limited number of samples collected at 4 L min^{-1} ($N = 4$; 2 at each station) constrains the resolution with which this result can be generalized.

At WACS Station 1, the Sea Sweep gPMA ($N = 8$) had a mean composition and standard deviation of 43 (±11)% hydroxyl, 43 (±10)% alkane, and 14 (±4)% amine functional groups. At WACS Station 2 ($N = 4$), the hydroxyl group fraction increased to 58 (±11)%, the alkane group fraction decreased to 29 (±11)%, and the amine fraction was quite similar at 12 (±1)%. A similar difference in composition was observed in the

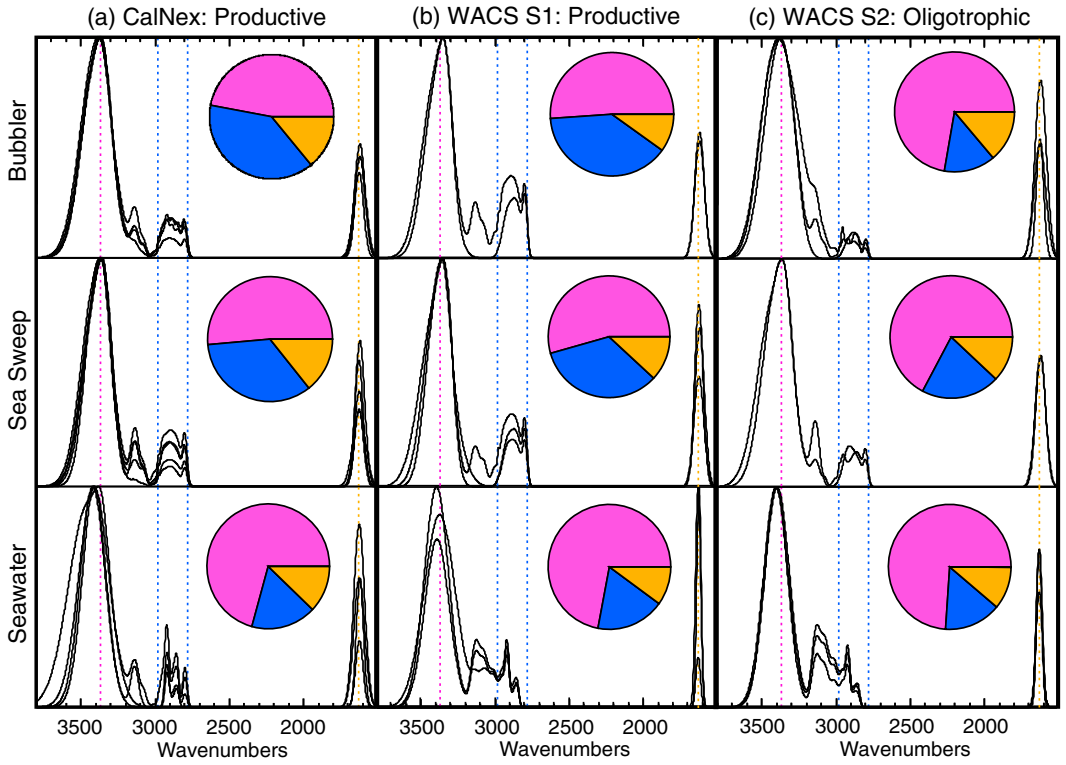

Figure 5. Comparison of the selected normalized organic FTIR spectra and average functional group composition measured at (a) CalNex, (b) WACS Station 1, and (c) WACS Station 2 in the gPMA generated with (top) the Bubbler, (middle) the Sea Sweep, and (bottom) the corresponding composition of OM in surface seawater. Pies represent the organic functional group composition as hydroxyl (pink), alkane (blue), and amine (orange). The dashed vertical lines indicate hydroxyl functional group peak absorption at 3369 cm^{-1} (pink) and amine functional group peak absorption at 1630 cm^{-1} (orange). The range of alkane functional group absorption from 2980 to 2780 cm^{-1} (blue dashed lines) is also shown. The higher wave number peak absorption of the hydroxyl functional groups is evident in the seawater panel. The functional group compositions and spectra are from the subset of collocated samples.

Bubbler gPMA for the two sampling regions, with a composition of 51 (±2)% hydroxyl, 39 (±3)% alkane, and 10 (±2)% amine groups at WACS Station 1 ($N = 2$) and 70 (±7)% hydroxyl, 18 (±8)% alkane, and 12 (±4)% amine at Station 2 ($N = 6$). During CalNex, the Sea Sweep gPMA ($N = 6$) had an average composition of 47 (±14)% hydroxyl, 38 (±13)% alkane, and 15 (±3)% amine functional groups, while the Bubbler gPMA ($N = 8$) had a composition of 42 (±9)% hydroxyl, 44 (±8)% alkane, and 14 (±3)% amine functional groups.

Bubbler and Sea Sweep gPMA samples that overlapped in time and location are compared for the two projects in Figure 5 (see section 7.3 in the supporting information for the samples selected). Using these collocated samples, at WACS Station 1, the Sea Sweep gPMA ($N = 3$) had a mean composition and standard deviation of 54 (±4)% hydroxyl, 34 (±3)% alkane, and 12 (±1)% amine functional groups. At WACS Station 2 ($N = 2$), the hydroxyl group fraction increased to 67 (±8)%, the alkane group fraction decreased to 21 (±7)%, and the amine fraction was quite similar at 12 (±1)%. The same difference in composition was observed in the Bubbler gPMA for the two sampling regions, with a composition of 51 (±2)% hydroxyl, 39 (±3)% alkane, and 10 (±2)% amine groups at WACS Station 1 ($N = 2$) and 73 (±6)% hydroxyl, 14 (±2)% alkane, and 14 (±4)% amine at Station 2 ($N = 3$). During CalNex, the Sea Sweep gPMA ($N = 5$) had an average composition of 51 (±10)% hydroxyl, 34 (±8)% alkane, and 14 (±3)% amine functional groups, while the Bubbler gPMA ($N = 4$) had a composition of 47 (±7)% hydroxyl, 39 (±7)% alkane, and 14 (±1)% amine functional groups.

The difference (42% versus 22%) in alkane group fraction of the combined Sea Sweep and Bubbler gPMA measured at WACS Station 1 and Station 2 is comparable to the variability (±9% and ±13%) at each station; the difference (35% versus 16%) is more significant when only the collocated samples at each station are compared as the variability for those samples is less (±6% and ±4%). The collocated samples may show local, short-term trends that are masked by averaging over the longer times and wider regions that were sampled

during the entire cruise. Hence, it is also true that for the wider range of seawater sampled by the entire 9 day cruise, the average Sea Sweep gPMA OM alkane fraction for the two stations were closer to each other than the variability that was sampled, as noted by *Quinn et al*. [2014]. Nonetheless, this investigation should be considered exploratory, as only 3 days of sampling at each site are not sufficient to establish whether these local differences are characteristic of broader temporal and spatial scales.

3.5. aMA and gPMA Single-Particle Compositions

STXM-NEXAFS spectra of aMA and gPMA single particles collected during WACS and CalNex were sorted into two OM types with those spectra containing oxidized groups (i.e., carboxylic carbonyl and alcohol) as a high O/C particle type and those containing only absorption in the alkyl region in the low O/C particle type (following the classification of *Frossard et al*. [2014]). The high O/C particles were further separated into those that contained spectral features and morphology similar to the polysaccharides on sea-salt particles observed by *Russell et al*. [2010] and *Hawkins and Russell* [2010] and those that were uniformly organic throughout the particle. The WACS aMA studied by STXM-NEXAFS consisted of 13 high O/C particles each associated with sea salt, 4 high O/C particles (without sea-salt contributions in the individual particles), and 1 low O/C particle (without sea salt). These particles had geometric diameters that ranged from 0.39 to 2.6 μm [*Frossard et al*., 2014]. Together, the Sea Sweep and Bubbler gPMA during WACS were made up of 29 high O/C particles and 25 low O/C particles.

3.6. Seawater OM Functional Group Composition

Seawater OM measured during CalNex ($N = 4$) and WACS Station 1 ($N = 3$) and Station 2 ($N = 3$) had similar mean compositions with 70 (±1)%, 72 (±6)%, and 74 (±2)% hydroxyl; 17 (±7)%, 18 (±3)%, and 15 (±2)% alkane; and 12 (±7)%, 10 (±7)%, and 11 (±1)% amine functional groups, respectively. The seawater OM samples collected during WACS Station 1 at 27.2 m ($N = 1$) and Station 2 at 2500 m ($N = 1$) are also similar in composition to the near-surface seawater (5 m), both with 69% hydroxyl, 16% alkane, and 15% amine functional groups. However, the limited number of deep seawater samples is insufficient to characterize the variability of seawater with depth.

4. Discussion

The aMA and gPMA measurements made in multiple ocean regions are used to determine the factors that contribute to the organic composition of aMA, including the influence of PMA. Three main questions are addressed: (i) what is the organic functional group composition of ocean-derived aMA? (ii) how much of aMA composition can be explained by generating primary marine aerosol (gPMA) from bubbled seawater? and (iii) what are the differences between the organic compositions of gPMA and seawater?

4.1. Chemical Composition of Ocean-Derived aMA: aPMA and CMA

The organic composition of aMA contains two ocean-derived or clean marine OM types (aPMA and CMA), based on the aMA classification in section 3.1 and the lack of fossil-fuel-related alkane functional group signatures. aPMA OM has a composition (Table 4) similar to the composition of saccharides as shown in Figure 6. In general, the organic compositions of the aPMA samples and saccharides all have hydroxyl functional group fractions greater than 55% and alkane functional group fractions less than 45% (with the specific ranges of saccharide alkane functional group fractions in Table S3 in the supporting information). The average FTIR spectrum of the aPMA OM samples has high average cosine similarities (all greater than 0.80) with saccharide spectra (Table S3 in the supporting information), indicating that aPMA composition is consistent with any of the saccharide standards or a mixture thereof, since the specific molecular mixture cannot be identified by FTIR. The aPMA OM-type spectra have a similar hydroxyl functional group peak location ($3377 \pm 44\ cm^{-1}$) to the monosaccharides ($3373 \pm 4\ cm^{-1}$) and disaccharides ($3383 \pm 4\ cm^{-1}$). While the average aPMA peak locations are more similar to those of the smaller saccharides (monosaccharides and disaccharides), the range of hydroxyl group peak locations for individual samples are also within the range of the polysaccharides ($3425 \pm 24\ cm^{-1}$), as shown in Table 5, indicating that the variability sampled is too large to identify the composition as either monosaccharides or disaccharides rather than polysaccharides. Likely it is a complex mixture of multiple compounds of both classes. This hydroxyl group peak location and overall composition are consistent with the previously identified polysaccharide-like composition of PMA OM [*Russell et al*., 2010]. However, the larger fraction of alkane functional groups in this aPMA OM

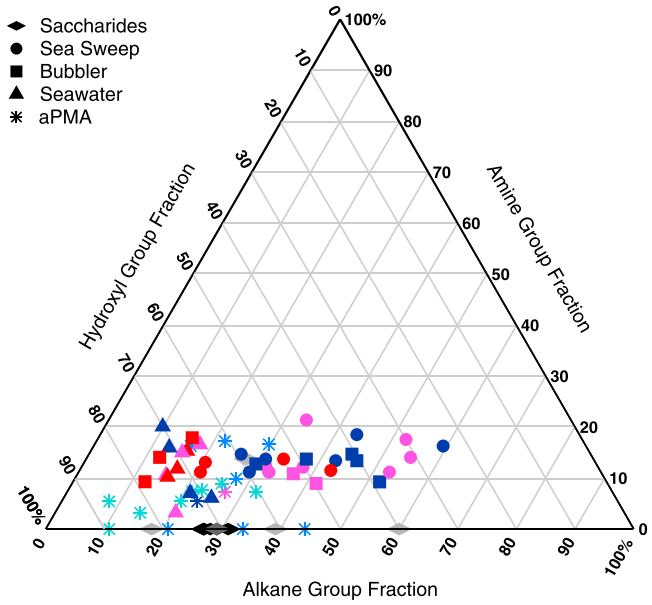

Figure 6. The hydroxyl, alkane, and amine functional group fractional compositions of gPMA, aPMA, seawater, and saccharide OM. Each marker represents an individual sample. Markers are colored based on the sample project and location for WACS Station 1 (pink), WACS Station 2 (red), EPEACE (light blue), CalNex (dark blue), and ICEALOT (teal). Saccharides are shown in grey diamonds as polysaccharides (light grey), disaccharides (grey), and monosaccharides (dark grey). For the aPMA particles, the hydroxyl group fraction includes carboxylic acid.

type (21 ± 9%) is likely more accurate than the 10–15% alkane group associated with the "marine factor" obtained by positive matrix factorization (PMF) [*Russell et al*., 2010], since the PMF results rely on the statistical separation of noncovarying factors in a time series that includes a sufficient number of unmixed aPMA samples.

The general composition, including the presence of amine functional groups, and the average spectrum of the aPMA OM are also similar to that of the polysaccharide chitosan, which is derived from the deacetylation of chitin, a constituent of the high-molecular-weight fraction of OM in seawater [*Aluwihare et al*., 2005]. Chitosan has a broad IR absorbance (peak at 3410 cm^{-1}) in the hydroxyl functional group region and IR absorbance at 1630 cm^{-1} in the amine functional group region, similar to the average aPMA OM spectrum, with absorption at 3377 and 1623 cm^{-1} (shown in Figure S2 and Table S3 in the supporting information). The functional group composition calculated from the molecular structure of chitosan contains 59% hydroxyl, 27% alkane, and 14% amine functional groups.

Additional amino sugars (monosaccharides) such as glucosamine and galactosamine have been observed in both seawater particulate organic matter (POM) and ultrafiltered seawater-dissolved organic matter (DOM) [*Benner and Kaiser*, 2003]. Another constituent of seawater OM is peptidoglycan, which has absorbance at 3300 and 1657 cm^{-1}, is a major component of bacteria cell walls, and contains one base compound (N-acetyl-glucosamine) in common with chitosan [*Naumann et al*., 1982]. The amine functional group fraction observed in the aPMA OM can also indicate the presence of amino acids. For example, the spectrum of the amino acid asparagine has an IR absorption bend of NH_2 at 1620 cm^{-1} [*Venyaminov and Kalnin*, 1990]. *Aminot and Kerouel* [2006] also measured dissolved free primary amines and amino acids in seawater, and amine carbons were observed in DOM by *Benner et al*. [1992]. Additionally, the molar ratios of C/N (Table 4) in the aPMA (9.8), gPMA (6.9), and seawater (8.0) OM are similar to the range of measured C/N in the cellular material of phytoplankton (8.8) [*Biersmith and Benner*, 1998] and slightly larger than that measured for samples of marine plankton and bacteria (6.3) [*Emerson and Hedges*, 2008] and demonstrated by the Redfield ratio (6.6). The similarity of the amine functional group fraction in gPMA and seawater is also consistent with recent measurements of seawater

Table 5. The Location of the Maximum Hydroxyl Group Peak (cm^{-1}) for Seawater, gPMA, aPMA, and Saccharides

OM Type	Hydroxyl Group Peak Location (cm^{-1})
Seawater	3401 ± 14
gPMA	3369 ± 10
Productive	3362 ± 7
Nonproductive	3376 ± 9
aPMA	3377 ± 44
Monosaccharides[a]	3373 ± 4
Disaccharides[b]	3383 ± 4
Polysaccharides[c]	3425 ± 24

[a]Glucose, fructose, xylose, and galactose.
[b]Lactose and cellobiose.
[c]Pectin, carboxymethyl cellulose, and chitosan.

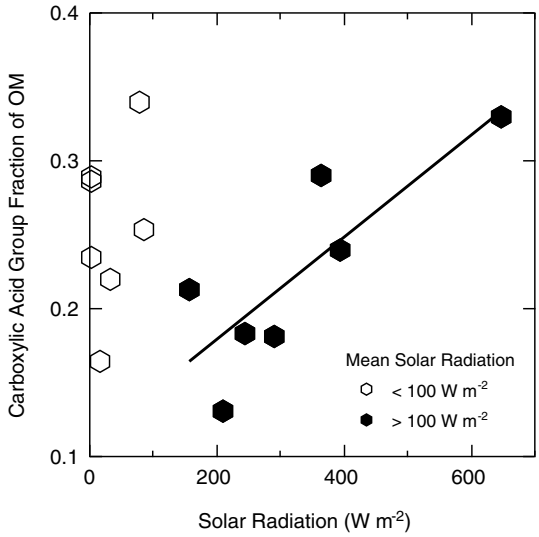

Figure 7. Correlation of the carboxylic acid functional group fraction of CMA OM (observed during EPEACE and ICEALOT) with solar radiation. A threshold of 100 W m^{-2} was used to exclude the samples in low light that were not likely to have OM dominated by local or recent photochemical production.

and gPMA that showed that nitrogen-containing organic compounds were present in similar, but slightly lower, proportions in gPMA compared to seawater [*Schmitt-Kopplin et al.*, 2012]. It is also worth noting that the measured amine functional groups can include the contributions of amide-containing molecules, since mild acid hydrolysis (as might occur during sample drying) under low-pH conditions can destroy the amide functional group bond linkage in seawater proteins and release amino acids, resulting in amine functional groups [*Aluwihare et al.*, 2005].

The other clean aMA OM is CMA (Table 4). Compared to the average aPMA OM spectrum, the average CMA OM spectrum has a hydroxyl functional group maximum absorbance at lower wavenumbers (3288 cm^{-1}), indicating that there is a difference in the bond structure of the two OM types (Figure 2). The shoulder in the CMA spectrum at higher wavenumbers (around 3385 cm^{-1}) is consistent with the hydroxyl group peak absorbance of the aPMA OM type (3377 ± 44 cm^{-1}), within the measurement variability, and is consistent with a substantial contribution of aPMA in CMA OM.

Carboxylic acid groups in CMA likely originate from the condensation of photochemical reaction products of volatile organic compounds (VOCs), which may be marine in origin, although oxidation or precursors in the particle phase can also contribute. *Turekian et al.* [2003] observed that both of these pathways were sources of oxalic acid in marine aerosol particles. *Zhou et al.* [2008] observed the photolysis of gPMA OM, which produced OH and hydroperoxides when exposed to solar radiation. Other studies have identified carboxylic acid functional groups as SOA based on correlation with solar radiation [*Rogge et al.*, 1993] and correlation with ozone [*Liu et al.*, 2011; *Satsumabayashi et al.*, 1990]. The carboxylic acid functional group fraction of the CMA OM is strongly correlated ($r = 0.82$) with solar radiation, for the samples with mean solar radiation (averaged over the sampling interval) greater than 100 W m^{-2} (Figure 7). The samples with mean values less than 100 W m^{-2} were excluded from the correlation because such low-light exposures during sampling meant that those samples were unlikely to have been influenced by local photochemical production and instead likely contained OM formed during prior sunlight exposure. This correlation is consistent with a photochemical source of the carboxylic acid group mass in CMA, providing a "secondary" contribution that is chemically distinct from the hydroxyl-alkane-amine group mixture associated with the primary components of aPMA.

The OC/Na^+ ratio of the aPMA OM type (0.45) is consistent with previously measured submicron PMA particles with OC/Na^+ ranging from 0.1 to 2 [*Russell et al.*, 2010, and references therein]. The higher ratio of OC/Na^+ (1.07) in CMA can be interpreted as an indicator of secondary contributions of the photochemical products of VOCs to particles in the atmosphere.

The O/C ratio for the aPMA OM type is 1.03 (±0.21). The O/C ratio of organic aerosol has been observed to increase over time after particles are emitted due to photochemical processing and secondary formation of organic components [*Aiken et al.*, 2008; *Zhang et al.*, 2005], and an O/C value higher than 0.4 is considered to be highly oxidized [*DeCarlo et al.*, 2008]. In marine conditions, the interpretation of high O/C as secondary is not appropriate since the large fraction of hydroxyl groups in saccharides means that even primary components have high O/C. The calculated O/C value for the monosaccharide reference standard glucose is 1.33, which is more than 3 times higher than O/C values attributed in nonmarine conditions as secondary (0.4). Nonetheless, the increase in the O/C ratio between the aPMA OM samples (0.80 ± 0.18) and the CMA OM (1.09 ± 0.17) samples in EPEACE is consistent with a larger secondary component in CMA relative to aPMA.

This observed increase in the fraction of carboxylic acid functional groups is consistent with the accumulation of LMW products such as dicarboxylic acids [*Kawamura and Sakaguchi*, 1999; *Zhou et al*., 2008]. The VOC precursors of these acids may be either marine or continental in origin, but the low amount of fossil fuel contributions in the particles is more consistent with a biogenic marine VOC source. More discussion of the presence of marine carboxylic acids is included in section 7.6 in the supporting information.

STXM-NEXAFS single-particle measurements of aMA also show the presence of carboxylic acid and oxidized functional groups in the atmosphere during WACS. Of the 18 aMA particles measured, 17 were classified as high O/C. This high fraction of more oxidized particles is consistent with the high carboxylic acid functional group fraction identified by FTIR in these samples.

4.2. Chemical Similarities Between gPMA and aPMA and Differences Between gPMA and Other aMA

The similarities of the organic composition of gPMA and aMA provide direct evidence for the sources of aMA and, specifically, the contribution of PMA to aMA. The differences between gPMA and non-ocean derived aMA (SMA and MMA) provide clear evidence for the contribution of nonmarine sources to particle OM over the ocean.

4.2.1. Similarities Between gPMA and aPMA

The comparison of the aPMA and gPMA (Figure 6) OM shows the similarities in the functional group compositions of OM of these two types. The average aPMA OM spectrum has cosine similarities of greater than 0.90 with the gPMA OM spectra. The gPMA OM spectra have similar hydroxyl group peak locations ($3369 \pm 10\ cm^{-1}$) to the aPMA spectra ($3377 \pm 44\ cm^{-1}$) as shown in Table 5. The average gPMA OM composition is also very similar to the aPMA composition (Table 4). Additionally, the OC/Na^+ ratio of the aPMA (0.45) falls within the range of gPMA (0.06–0.6) measured during WACS. This similarity in organic composition between aPMA and gPMA provides evidence that the aPMA is ocean derived, likely produced through a bubble bursting mechanism similar to that of gPMA, supporting both the assertion that most aPMA OM is directly emitted in the particle phase from the ocean to the atmosphere and the utility of the Sea Sweep and Bubbler in generating gPMA that is, in key respects, similar to aPMA. Also, as discussed earlier for aPMA, the average functional group composition of gPMA is quite similar to that of the amino sugar chitosan, a seawater constituent.

4.2.2. Differences Between gPMA and Non-Ocean-Derived OM in aMA

Some of the marine samples selected by the three aMA criteria still retain the chemical signatures of shipping and other marine pollution in their FTIR spectra. This is evident in the SMA (Figure 2c) and MMA (Figure 2d) OM types in which the alkane peak absorption is similar to that of fossil fuel emissions [*Guzman-Morales et al*., 2013]. These two OM types make up 63% of the total measured aMA OM concentration, consistent with the near ubiquity of black carbon (BC) measured in the southeastern Pacific [*Shank et al*., 2012]. Even though these types show chemical components characteristic of anthropogenic sources, the quantitative contributions are sufficiently dilute that the average SMA and MMA OM concentration is only $0.55\ \mu g\ m^{-3}$ (with more than 80% of the sample concentrations less than $1\ \mu g\ m^{-3}$), concentrations that many classification schemes would consider clean. In addition, these low concentrations are not excluded by filters triggered by the high particle counts (e.g., $>1000\ cm^{-3}$) that are associated with nearby sources, since the emissions have been diluted by mixing with cleaner air in the boundary layer.

Cloud droplet composition measurements off the coast of central California, where 16 of the 18 SMA OM samples were collected, show that 72% of the cloud droplets in that area are at least moderately perturbed by shipping emissions [*Coggon et al*., 2012]. Additionally, a major shipping lane between the port of San Francisco and the Southern California ports transits through the area sampled during EPEACE. The factor of 2–3 higher alkane functional group mass fraction ($66 \pm 6\%$) in SMA OM, compared to the clean aMA (aPMA with $21 \pm 9\%$ and CMA with $24 \pm 7\%$), is likely due to shipping emissions.

The MMA OM type has a high ratio of OC/Na^+ (greater than 5) suggesting that a substantial fraction of the OC is not primary OC from seawater. These samples also have the highest average corresponding solar radiation, which could increase the contribution of photochemical products of VOCs to the OC. The fraction of carboxylic acid functional groups is consistent with this result [*Liu et al*., 2011], but there is no strong correlation of the carboxylic acid fraction with solar radiation, indicating that the carboxylic acid functional groups may have been transported from elsewhere rather than forming recently. It is interesting that the

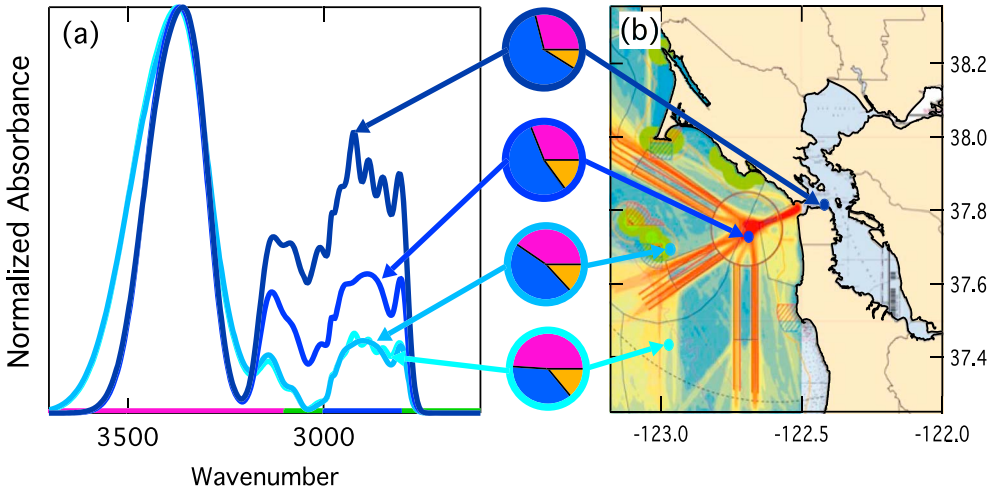

Figure 8. (a) Normalized FTIR spectra of Bubbler gPMA generated at 4.2 L min^{-1} at four locations starting outside (light blue) and ending in (dark blue) the San Francisco Bay. (b) Map of the locations where gPMA were generated overlaid on a map of shipping lanes (red) into the San Francisco Bay (source: http://www.calacademy.org/sciencetoday/shipping-lane-changes/5511420/). The pies represent the functional group composition of the gPMA OM at the four locations with alkane (blue), hydroxyl (pink), and amine (orange) functional groups.

composition of MMA is quite similar in multiple ocean regions, reflecting the general chemical similarity of both shipping fuel and ocean components across different parts of the world.

4.2.3. Shipping Effluent Signatures in gPMA

A striking example of how gPMA can also incorporate nonnatural seawater components was identified during CalNex in seawater that contained increasing amounts of fuels. The alkane functional group fraction of the gPMA OM increased as the R/V *Atlantis* proceeded into the shipping lanes and into the bay (Figure 8b). The gPMA OM in the bay had a much higher fraction of alkane functional groups (62%) than the gPMA farthest outside of the bay (37%). Since the gPMA do not have any contributions from atmospheric processes, the observed change in the alkane functional group fraction results from changes in the seawater organic composition. A likely explanation is that the shipping lanes contribute more fuel waste to the bay, resulting in seawater with a higher alkane group fraction and corresponding higher fractions in the bubbled gPMA. Additional sources of hydrocarbons, such as coastal runoff into the bay, may also increase the seawater hydrocarbon content. Also, increased surfactants in the seawater in the bay may contribute to the larger alkane fraction of the gPMA, consistent with the mechanism discussed in section 4.3.3.

This link between changes in seawater composition and PMA has been seen in the associated aMA in previous studies. *Bahadur et al.* [2010] reported a unique link between the high-lignin waterways of the St. Lawrence and the aMA measured in the western north Atlantic. A study in Leghorn harbor showed evidence for ship fuel signatures in aMA measured in that region [*Cincinelli et al.*, 2001]. However, in those studies, the influence of atmospheric processing could not be ruled out, the way it can be here by observing the alkane fraction of gPMA. We also note that the alkane functional group peaks of the FTIR spectra for the fuel and ship-influenced marine type (Figure 2c) are very similar to those for the San Francisco Bay gPMA (Figure 8a), both with peaks at 2923 and 2804 cm^{-1}. This similarity means that seawater and atmospheric contributions to the alkane group components cannot be separated in aMA, except by comparison to gPMA.

4.3. Influence of Seawater OM on gPMA OM

Collecting seawater and gPMA in the same regions reveals a very strong relationship between the composition of seawater and the gPMA produced from it across three very different ocean regions. In general, gPMA OM composition is similar to seawater OM composition, but there are two main differences discussed below.

4.3.1. Spectral Similarities and Differences Between gPMA and Seawater

Seawater OM and gPMA OM have similar FTIR spectra and functional group compositions (Figure 6), both with large fractions (50–75%) of hydroxyl functional groups and smaller contributions from alkane groups

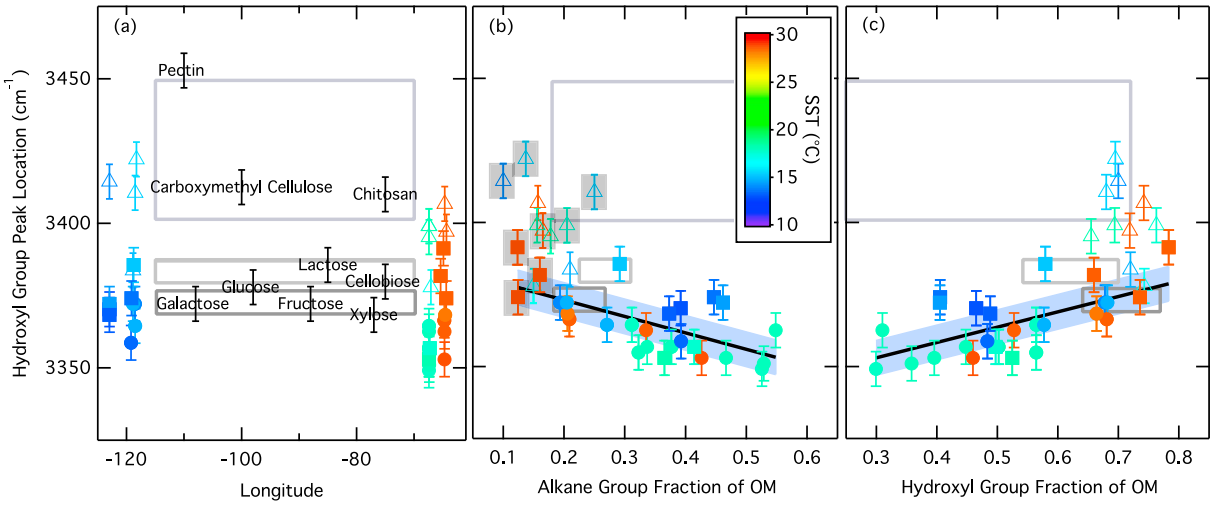

Figure 9. Comparison of maximum hydroxyl functional group peak location with (a) sample longitude, (b) alkane functional group fraction of OM, and (c) hydroxyl functional group fraction of OM for the gPMA and seawater. The marker shapes indicate the sample type including Sea Sweep (circles), Bubbler (squares), and seawater (open triangles). The saccharides are plotted at different longitudes for comparison in Figure 9a and at their corresponding molecular alkane and hydroxyl functional group fractions in Figures 9b and 9c, respectively. The large open grey boxes represent the average range of hydroxyl group peak absorption (average ± standard deviation) for polysaccharides (light grey), disaccharides (grey), and monosaccharides (dark grey). Error bars of ±6 cm^{-1} are shown for the hydroxyl group peak location on each marker to represent the method error. The uncertainty in the alkane and hydroxyl functional group mass is 20% [*Russell*, 2003]. The shaded boxes around individual markers (3 Bubbler and 5 seawater samples) are samples where the alkane functional group mass is above the detection limit but below the limit of quantification (twice the standard deviation), making the alkane mass fraction have an uncertainty of >50% rather than 20%. gPMA hydroxyl group peak location correlates with the alkane functional group fraction ($r = -0.65$) and the hydroxyl functional group fraction ($r = 0.63$).

(15–40%) and amine groups (5–20%). The OM spectra of the collocated gPMA and seawater samples are shown in Figure 5, and the ranges of hydroxyl group and alkane group fractions of all the gPMA samples and seawater are shown in Figure 6. This graph also illustrates that the hydroxyl and alkane group fractions of the measured seawater and gPMA are within the ranges expected for saccharides identified in seawater (polysaccharides 18–60% alkane groups and monosaccharides and disaccharides 19–31% alkane groups).

One subtle but interesting difference between seawater and gPMA is shown in the average hydroxyl functional group peak location listed in Table 5 and shown in Figure 5. The broad seawater hydroxyl functional group absorption region overlaps that of the gPMA OM spectra (Figure 5); this similarity is consistent with seawater being the source of gPMA. The general location of the hydroxyl group peak is consistent with known seawater saccharides, such as chitosan (see section 7.5 and Figure S2 in the supporting information). However, the specific hydroxyl functional group peak locations differ between the gPMA and seawater OM, with gPMA peaking at 3369 and seawater peaking at 3401 cm^{-1} (Table 5). This 32 cm^{-1} average difference in peak location is larger than the measured variability (±10 for gPMA and ±14 for seawater) and the method error (±6 cm^{-1}). Consequently the difference in peak location could indicate a systematic difference in the molecular structure and in the mixture of the saccharides in the seawater and the gPMA, since peak location shifts to higher wavenumbers for larger saccharides [*Mathlouthi and Koenig*, 1986; *Kuhn*, 1950]. The hydroxyl group peak location of the gPMA (3369 ± 10 cm^{-1}) is more characteristic of the measured monosaccharide (3373 ± 4 cm^{-1}) and disaccharide (3383 ± 4 cm^{-1}) molecules, than the seawater hydroxyl group peak location (3401 ± 14 cm^{-1}), which is more characteristic of polysaccharide (3425 ± 24 cm^{-1}) molecules (Figure 9a). While the complexity of the mixture of saccharides that are present in both seawater and gPMA clearly prevents a specific molecular identification, this shift in peak location may reveal differences in the relative contributions from different saccharide types.

The hydroxyl functional group peak locations measured in these samples are not correlated ($r < 0.4$) to SST, salinity, chl *a* concentration, or insolation and also are not region specific. The one factor that seems related to the hydroxyl functional group peak location in gPMA is the functional group composition of the OM, with a negative correlation to the alkane functional group fraction ($r = -0.65$) and a complementary positive correlation with the hydroxyl functional group fraction ($r = 0.63$) (Figure 9). The hydroxyl functional group peak location decreases as the hydroxyl group fraction decreases and the alkane group fraction increases.

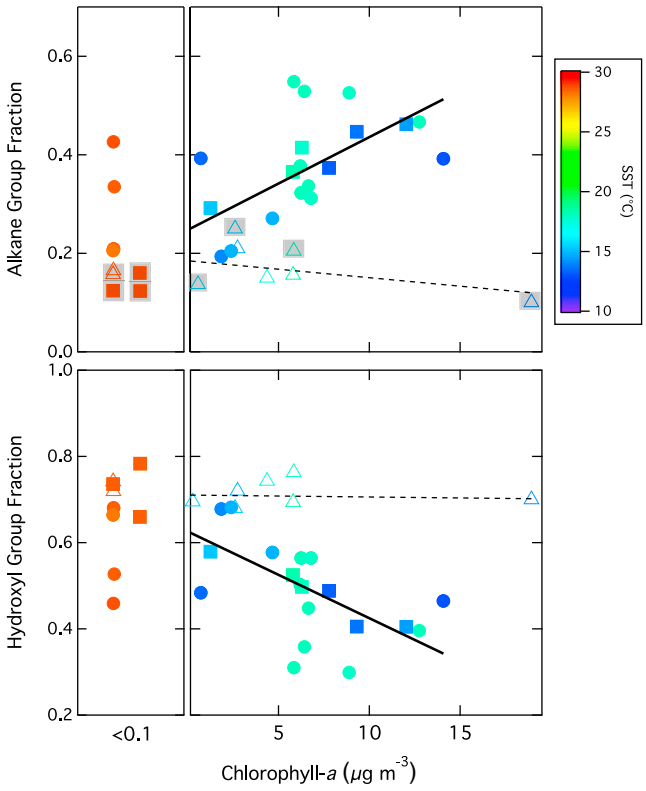

Figure 10. (a) Correlation of alkane functional group fraction of gPMA OM with seawater chl *a* concentrations ($r = 0.66$) and (b) negative correlation of hydroxyl functional group fraction of gPMA OM with seawater chl *a* concentrations ($r = -0.67$) during WACS and CalNex (over the range of chl *a* concentrations measured in this study). The markers represent sample types as Sea Sweep (circles), Bubbler (squares), and seawater (open triangles). The seawater alkane and hydroxyl functional group OM fractions do not correlate with chl *a* concentrations, indicated with the dashed lines. The shaded boxes around individual markers (3 Bubbler and 5 seawater samples) are samples where the alkane functional group mass is above the detection limit but below the limit of quantification (twice the standard deviation), making the alkane mass fraction have an uncertainty of >50% rather than 20%.

4.3.2. Chl *a*-Dependent Enhancement of Alkane Group Fraction in gPMA

Chl *a* concentration is used as a measure of biological activity (phytoplankton biomass) in the surface ocean, and high biological activity, as observed in productive regions with high concentrations of chl *a*, may affect the organic composition of aMA [*O'Dowd et al.*, 2004]. The alkane group fraction of the OM in gPMA particles is correlated with the chl *a* concentration ($r = 0.66$) over the range measured in this study (Figure 10a). Consequently, the hydroxyl functional group fraction of gPMA is negatively correlated with the chl *a* concentration ($r = -0.67$; Figure 10b). Together, the Sea Sweep and Bubbler-generated gPMA suggest a difference between the OM composition of gPMA from productive and nonproductive seawater (Table 4), indicated by high and low seawater chl *a* concentrations, respectively. There is a consistently higher fraction of alkane functional groups in the gPMA from the productive seawater of CalNex and WACS Station 1 ($42 \pm 9\%$) than from the nonproductive seawater at WACS Station 2 ($22 \pm 10\%$). As discussed above, longer time series of measurements in a broad range of ocean conditions are needed to confirm this result.

The average composition of the surface seawater OM in the productive and nonproductive seawater is fairly similar, which is consistent with measurements that found no significant differences in seawater film composition (including inorganic and organic components) in eutrophic and oligotrophic seawater [*Williams et al.*, 1986]. At WACS Station 1, seawater was also collected at a depth of 27.2 m, and at WACS Station 2, seawater was collected at a depth of 2500 m. The OM in these samples is similar to the surface seawater composition, with a variation of less than 5%.

These differences in gPMA OM composition between the productive and nonproductive seawater during WACS are also observed in the single-particle types measured by STXM-NEXAFS. In the productive seawater, there were 6 high O/C particles and 9 low O/C particles with diameters of 0.65 to 1.5 μm, while in the nonproductive seawater, there were 12 high O/C and 7 low O/C particles measured with diameters less than 1.5 μm. While the small number of particles analyzed by STXM-NEXAFS was selected based on carbon content and may not be representative of the entire OM particle population, these measurements indicate that there may be a higher fraction of low O/C particles in the gPMA from the productive seawater. This is in agreement with the larger fraction of alkane functional groups measured by FTIR in the gPMA generated in the productive seawater compared to the oligotrophic seawater.

Additionally, the alkane group fraction of PMA calculated using a classical Langmuir theory model, combined with estimates of ocean distributions of several classes of chemical compounds [*Burrows et al.*, 2014], correlates with chl *a* concentration. The model posits that a group of primarily aliphatic, lipid-like

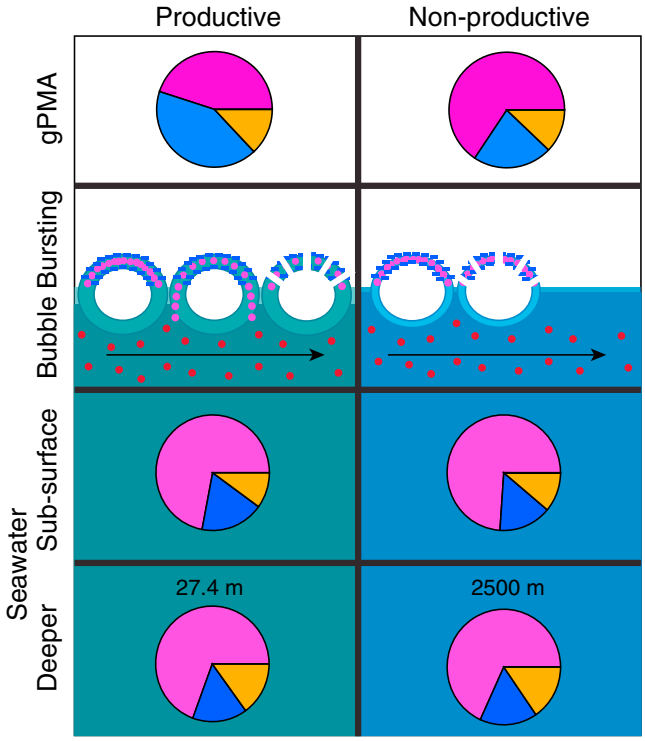

Figure 11. Average functional group composition of OM in (top) gPMA generated with the Sea Sweep and Bubbler, (middle) surface seawater, and (bottom) deep seawater at 27.4 m and 2500 m measured in (left column) productive and (right column) nonproductive seawater during WACS. The colors in the pies represent the organic functional group fractions for hydroxyl (pink), alkane (blue), and amine (orange). The bubbles show the bubble draining process in both seawater types, with more surfactant in the productive seawater. The OM is shown as hydrophobic (blue squares), hydrophilic (pink circles), and polysaccharides (red circles).

compounds is present in concentrations that are correlated with chl *a* and that this group outcompetes other molecules for inclusion in the bubble film due to its strong surface affinity. The direction of the model-predicted chl *a* to alkane group fraction relationship is the same as observed in this study, even though the model does not fully reflect the scale of the observed values. The same model also predicts a lack of correlation between the predicted seawater OM alkane group fraction and the seawater chl *a* concentration, similar to this study. These similar trends suggest consistency between the measurements and the classical Langmuir theory model.

4.3.3. Proposed Explanations for the Retention of Polysaccharide-Like OM in Seawater and the Enhancement of Alkane Groups in gPMA

Here we consider the processes by which the OM composition from seawater changes as particles form from bubbles bursting in seawater. Two processes are needed to explain the observations of (i) the similarity of gPMA to monosaccharide and disaccharide OM and (ii) the relative enhancement of alkane functional groups in gPMA. These are summarized in Figure 11 and are discussed below.

The retention of polysaccharide-like OM in the seawater, resulting in its depletion relative to monosaccharide and disaccharide-like OM in gPMA, is likely the result of the polysaccharide-like OM not being incorporated into the bubble films that produce particles. One possible explanation for this preferential partitioning is that polysaccharides can form transparent exopolymer gels in the surface microlayer [*Wurl and Holmes*, 2008; *Verdugo et al*., 2004; *Decho*, 1990], and such colloidal structures could prevent their inclusion in the bubble films and consequently their partitioning in the aerosol phase. Previous studies [*Bigg and Leck*, 2008; *Leck and Bigg*, 2005] have observed polysaccharide gels in marine aerosol, but it is possible that there is proportionally less polysaccharide-like OM in the aerosol than in the seawater. Another possible explanation is that polysaccharides could be cleaved by ultraviolet radiation at the sea surface [*Orellana and Verdugo*, 2003], reducing the abundance of polysaccharides available at the sea surface to contribute to the films that make aerosol particles.

The samples taken in productive seawater have higher concentrations of chl *a* (Table 3), indicative of higher phytoplankton concentrations, which have been associated with increased surfactant concentrations [*Zutic et al*., 1981; *Sellegri et al*., 2006; *Wurl et al*., 2011]. This connection provides the opportunity to use chl *a* as a proxy for surfactant concentrations. Even though the organic functional group composition of seawater is the same in productive and nonproductive seawater, the chl *a* concentrations are different and that small (below detection limit) change in organic composition is sufficient to account for substantial changes in surfactant properties of the seawater [*Modini et al*., 2013]. Higher concentrations of surfactants increase bubble persistence at the seawater surface before bursting [*Sellegri et al*., 2006], as observed with individual bubbles in the laboratory [*Modini et al*., 2013]. The longer bubbles persist, the more the bubble films are allowed to drain [*Blanchard*, 1963], so an increase in persistence time leads to additional drainage

from the films. Since the more soluble constituents of the bubble film drain more than the less soluble ones, the compounds with higher fractions of hydroxyl groups preferentially drain from the bubble film leaving the more insoluble organic compounds (including molecules with higher fractions of alkane groups) [*Oppo et al*., 1999; *Russell et al*., 2010]. The result is that the bubble films that form in productive seawater have a larger fraction of alkane groups by the time the bubble film ruptures, which then forms PMA particles that are enriched in alkane groups. Figure 11 illustrates this process of preferential draining of the more soluble molecules and the resulting enrichment of the alkane group fraction in the gPMA OM generated from productive seawater. This process is similar to the draining proposed by *Facchini et al*. [2010], in support of their finding that water-insoluble organic components were enhanced in gPMA.

5. Conclusions

The organic functional group composition of aMA (defined as particles collected more than 1 km from land and sampled in air masses with 3 day back trajectories originating over the open ocean) in five ocean regions including the northern Atlantic, Arctic, southeastern Pacific, and northeastern Pacific, both coastal and remote, was determined by FTIR spectroscopy and independent variables (sea salt, solar radiation, etc.) to have contributions from both clean and polluted sources. Ocean-derived organic aMA included atmospheric primary marine aerosol particles (aPMA) and carboxylic acid-enriched primary marine aerosol particles (CMA), which had average OM concentrations of 0.45 and 0.68 $\mu g\,m^{-3}$ and represented 23% and 14% of the total sampling time, respectively. Shipping-influenced marine aerosol particles (SMA) and mixed marine aerosol particle (MMA) OM accounted for 63% of the sampling time with a total aMA average OM of 0.55 $\mu g\,m^{-3}$ observed in four of the five sampling regions, confirming the ubiquitous contribution of nonnatural sources to aerosol particles in the MBL.

The average (and variability indicated as one standard deviation) functional group composition of aPMA OM is 65 (±12)% hydroxyl, 21 (±9)% alkane, 6 (±6)% amine, and 7 (±8)% carboxylic acid functional groups, similar to an overall molecular composition of marine saccharides and amino sugars, such as chitosan and glucosamine, which contain 59% hydroxyl, 27% alkane, and 14% amine functional groups. aPMA was measured during high wind speeds, had a high corresponding concentration of sea salt (OC/Na^+ of 0.45), and showed a correlation between corresponding Na^+ concentration and wind speed ($r = 0.70$), all indicative of a primary, ocean-derived source of OM. The aPMA OM is similar in composition to the gPMA OM generated from the Bubbler and the Sea Sweep (55 ± 14% hydroxyl, 32 ± 14% alkane, and 13 ± 3% amine functional groups). This shows that aPMA is dominated by direct, primary emissions from seawater, making primary emissions from seawater an important source of organics to the MBL, with aPMA measured during 23% of the sampling time.

The other ocean-derived OM type CMA contains 49 (±6)% hydroxyl, 24 (±7)% alkane, 4 (±4)% amine, and 22 (±6)% carboxylic acid functional groups. The relative increase in the carboxylic acid functional group fraction, compared to the aPMA (7 ± 8%), is likely the result of contributions from photochemical oxidation in the atmosphere to form secondary products with carboxylic acid functional groups. This is shown by the correlation ($r = 0.73$) of the carboxylic acid functional group fraction of CMA OM with solar radiation for samples with solar radiation greater than 100 $W\,m^{-2}$.

The organic functional group composition of gPMA directly follows changes in seawater organic composition. One example of this was observed in the increase in the alkane functional group fraction of gPMA generated in the San Francisco Bay and shipping lanes (62%) compared to the gPMA farthest outside of the bay (37%). The higher-traffic shipping lanes contribute fuel waste to the bay, which results in a higher alkane functional group fraction in the seawater OM and corresponding gPMA.

Even though the organic composition of the seawater OM and gPMA contain the same functional groups (hydroxyl, alkane, and amine) in nearly the same proportions, there is a difference in the saccharide compositions of the gPMA and seawater OM, which is evident in the differences in the hydroxyl group peak locations of their spectra. The hydroxyl group peak location of the gPMA (3369 ± 10 cm^{-1}) is similar to monosaccharide and disaccharide molecules (3373 ± 4 and 3383 ± 4 cm^{-1}, respectively) within the measured variability (4–10 cm^{-1}) and the method error (±6 cm^{-1}). The seawater OM hydroxyl group peak location is at higher wavenumbers (3401 ± 14 cm^{-1}) and is consistent with having more polysaccharide contributions

(hydroxyl group peak location of $3425 \pm 24\ cm^{-1}$). The difference between the seawater and gPMA OM, demonstrated by the differences in their hydroxyl group peak locations ($3401 \pm 14\ cm^{-1}$ and $3369 \pm 10\ cm^{-1}$, respectively), results from the more polysaccharide-like OM remaining in the seawater during gPMA production. However, given the variability in the peak locations, a larger number of samples would be needed to identify the extent of the chemical difference between seawater and gPMA.

One other chemical difference is that the gPMA OM composition had a larger fraction of alkane functional groups when generated in eutrophic, productive seawater ($42 \pm 9\%$) compared to oligotrophic, nonproductive seawater ($22 \pm 10\%$). The gPMA organic functional group composition variation was not the result of a seawater organic functional group change, since the seawater alkane functional group fraction was consistently around 17% in both the productive and nonproductive regions. The difference in the gPMA from productive and nonproductive seawater may be the result of a change in the seawater surfactant concentration identified by the difference in chl *a* concentrations. The correlation ($r = 0.66$) between the gPMA alkane functional group fraction of OM and chl *a* concentration suggests that the alkane functional group fraction of gPMA may be directly related to the chl *a* concentration, suggesting a link between the ocean ecosystem biotic population and the aerosol composition. The difference may be a result of the higher concentration of surfactants (and chl *a*) in the productive seawater, which could increase the persistence time of the bubbles and allow for more draining of the soluble organics, including those with hydroxyl functional groups, from the bubble film before bursting. This process could result in a larger fraction of alkane functional groups in the bursting bubble film OM and the resulting gPMA from productive seawater than from nonproductive seawater. Further measurements are needed to test this hypothesis.

Acknowledgments

This work was funded by NSF grants AGS-1013423, OCE-1129580, and AGS-1360645. PNNL acknowledges additional support from the Office of Science Biological and Environmental Research Program of the U.S. Department of Energy as part of the Earth System Modeling Program. The authors thank William Keene at the University of Virginia and David Kieber at the State University of New York at Syracuse for deploying the Bubbler during CalNex and WACS and for the use of the data collected with the Bubbler. The authors thank the captains, crews, and scientists onboard the R/V *Knorr*, *Ronald H. Brown*, *Atlantis*, and *Point Sur* for their support in the field. The authors also thank Derek Coffman, Drew Hamilton, John Maben, Michael Long, Lelia Hawkins, Janin Guzman-Morales, Anita Johnson, and Robin Modini for their assistance with sample collection. The authors acknowledge Grace Weissner, Randelle Bundy, and Katherine Barbeau for running calibrations, providing training, and lending the fluorometer for chl *a* concentration measurements for the EPEACE samples. They also acknowledge David Kilcoyne at the Lawrence Berkeley National Laboratory Advanced Light Source and Satoshi Takahama for his assistance with STXM-NEXAFS and beamline operation. To obtain the data used in this study, please contact the corresponding author (lmrussell@ucsd.edu) or visit http://aerosol.ucsd.edu/papers/MarineOMdata.zip and http://saga.pmel.noaa.gov/data.

References

Aiken, A. C., et al. (2008), O/C and OM/OC ratios of primary, secondary, and ambient organic aerosols with high-resolution time-of-flight aerosol mass spectrometry, *Environ. Sci. Technol.*, *42*(12), 4478–4485, doi:10.1021/es703009q.

Aluwihare, L. I., and D. J. Repeta (1999), A comparison of the chemical characteristics of oceanic DOM and extracellular DOM produced by marine algae, *Mar. Ecol. Prog. Ser.*, *186*, 105–117.

Aluwihare, L. I., D. J. Repeta, and R. F. Chen (1997), A major biopolymeric component to dissolved organic carbon in surface sea water, *Nature*, *387*(6629), 166–169.

Aluwihare, L. I., D. J. Repeta, S. Pantoja, and C. G. Johnson (2005), Two chemically distinct pools of organic nitrogen accumulate in the ocean, *Science*, *308*(5724), 1007–1010, doi:10.1126/science.1108925.

Aminot, A., and R. Kerouel (2006), The determination of total dissolved free primary amines in seawater: Critical factors, optimized procedure and artefact correction, *Mar. Chem.*, *98*(2–4), 223–240, doi:10.1016/j.marchem.2005.07.005.

Ault, A. P., D. F. Zhao, C. J. Ebben, M. J. Tauber, F. M. Geiger, K. A. Prather, and V. H. Grassian (2013), Raman microscpectroscopy and vibrational sum frequency generation spectroscopy as probles of the bulk and surface compositions of size-resolved sea spray particles, *Phys. Chem. Chem. Phys.*, *15*(17), 6206–6214.

Bahadur, R., T. Uplinger, L. M. Russell, B. C. Sive, S. S. Cliff, D. B. Millet, A. Goldstein, and T. S. Bates (2010), Phenol Groups in Northeastern US Submicrometer Aerosol Particles Produced from Seawater Sources, *Environ. Sci. Technol.*, *44*(7), 2542–2548, doi:10.1021/es9032277.

Bates, T. S., D. J. Coffman, D. S. Covert, and P. K. Quinn (2002), Regional marine boundary layer aerosol size distributions in the Indian, Atlantic, and Pacific Oceans: A comparison of INDOEX measurements with ACE-1, ACE-2, and Aerosols99, *J. Geophys. Res.*, *107*(D19), 8026, doi:10.1029/2001JD001174.

Bates, T. S., et al. (2012), Measurements of Ocean Derived Aerosol off the Coast of California, *J. Geophys. Res.*, *117*, D00V15, doi:10.1029/2012JD017588.

Benner, R., and K. Kaiser (2003), Abundance of amino sugars and peptidoglycan in marine particulate and dissolved organic matter, *Limnol. Oceanogr.*, *48*(1), 118–128.

Benner, R., J. D. Pakulski, M. McCarthy, J. I. Hedges, and P. G. Hatcher (1992), Bulk chemical characteristics of dissolved organic-matter in the ocean, *Science*, *255*(5051), 1561–1564.

Biersmith, A., and R. Benner (1998), Carbohydrates in phytoplankton and freshly produced dissolved organic matter, *Mar. Chem.*, *63*(1–2), 131–144.

Bigg, E. K. (2007), Sources, nature and influence on climate of marine airborne particles, *Environ. Chem.*, *4*(3), 155–161, doi:10.1071/en07001.

Bigg, E. K., and C. Leck (2008), The composition of fragments of bubbles bursting at the ocean surface, *J. Geophys. Res.*, *113*, D11209, doi:10.1029/2007JD009078.

Blanchard, D. C. (1963), The electrification of the atmosphere by particles from bubbles in the sea, *Prog. Oceanogr.*, *1*(48), 16–16.

Blanchard, D. C. (1964), Sea-to-air transport of surface active material, *Science*, *146*(364), 396–397.

Blanchard, D. C., and A. H. Woodcock (1980), The production, concentration, and vertical distribution of the sea-salt aerosol, *Ann. N. Y. Acad. Sci.*, *338*(1), 330–347.

Burrows, S. M., O. Ogunro, A. A. Frossard, L. M. Russell, P. J. Rasch, and S. Elliott (2014), A Physically-based Framework for Modelling the Organic Fractionation of Sea Spray Aerosol from Bubble Film Langmuir Equilibria, *Atmos. Chem. Phys. Discuss.*, *14*, 5375–5443, doi:10.5194/acpd-14-5375-2014.

Buseck, P. R., and M. Posfai (1999), Airborne minerals and related aerosol particles: Effects on climate and the environment, *Proc. Natl. Acad. Sci. U.S.A.*, *96*(7), 3372–3379, doi:10.1073/pnas.96.7.3372.

Cavalli, F., et al. (2004), Advances in characterization of size-resolved organic matter in marine aerosol over the North Atlantic, *J Geophys. Res*, *109*, D24215, doi:10.1029/2004JD005137.

Ceburnis, D., C. D. O'Dowd, G. S. Jennings, M. C. Facchini, L. Emblico, S. Decesari, S. Fuzzi, and J. Sakalys (2008), Marine aerosol chemistry gradients: Elucidating primary and secondary processes and fluxes, *Geophys. Res. Lett.*, *35*, L07804, doi:10.1029/2008GL033462.

Ceburnis, D., et al. (2011), Quantification of the carbonaceous matter origin in submicron marine aerosol by C-13 and C-14 isotope analysis, *Atmos. Chem. Phys.*, *11*(16), 8593–8606, doi:10.5194/acp-11-8593-2011.

Cincinelli, A., A. M. Stortini, M. Perugini, L. Checchini, and L. Lepri (2001), Organic pollutants in sea-surface microlayer and aerosol in the coastal environment of Leghorn - (Tyrrhenian Sea), *Mar. Chem.*, *76*(1–2), 77–98, doi:10.1016/s0304-4203(01)00049-4.

Clarke, A. D., S. R. Owens, and J. C. Zhou (2006), An ultrafine sea-salt flux from breaking waves: Implications for cloud condensation nuclei in the remote marine atmosphere, *J. Geophys. Res.*, *111*, D06202, doi:10.1029/2005JD006565.

Coggon, M. M., et al. (2012), Ship impacts on the marine atmosphere: Insights into the contribution of shipping emissions to the properties of marine aerosol and clouds, *Atmos. Chem. Phys.*, *12*(18), doi:10.5194/acp-12-8439-2012.

Collins, D. B., et al. (2014), Direct aerosol chemical composition measurements to evaluate the physicochemical differences between controlled sea spray aerosol generation schemes, *Atmos. Meas. Tech. Discuss.*, *7*, 6457–6499, doi:10.5194/amt-7-1-2014.

Crahan, K. K., D. A. Hegg, D. S. Covert, H. Jonsson, J. S. Reid, D. Khelif, and B. J. Brooks (2004), Speciation of organic aerosols in the tropical mid-pacific and their relationship to light scattering, *J. Atmos. Sci.*, *61*(21), 2544–2558.

DeCarlo, P. F., et al. (2008), Fast airborne aerosol size and chemistry measurements above Mexico City and Central Mexico during the MILAGRO campaign, *Atmos. Chem. Phys.*, *8*(14), 4027–4048.

Decesari, S., et al. (2011), Primary and secondary marine organic aerosols over the North Atlantic Ocean during the MAP experiment, *J. Geophys. Res.*, *116*, D22210, doi:10.1029/2011JD016204.

Decho, A. W. (1990), Microbial exopolymer secretions in ocean environments: their role(s) in food webs and marine processes, *Oceanogr. Mar. Biol.*, *28*, 73–153.

de Leeuw, G., E. L. Andreas, M. D. Anguelova, C. W. Fairall, E. R. Lewis, C. O'Dowd, M. Schulz, and S. E. Schwartz (2011), Production flux of sea spray aerosol, *Rev. Geophys.*, *49*, RG2001, doi:10.1029/2010RG000349.

Draxler, R. R., and G. D. Rolph (2003), HYSPLIT (HYbrid Single-Particle Lagrangian Integrated Trajectory), Air Resources Laboratory, NOAA, Silver Spring, Md., (Model access via NOAA ARL READY Website. [Available at http://www.arl.noaa.gov/readyhysplit4.html).]

Druffel, E. R. M., P. M. Williams, J. E. Bauer, and J. R. Ertel (1992), Cycling of dissolved and particulate organic-matter in the open ocean, *J. Geophys. Res.*, *97*(C10), 15,639–15,659, doi:10.1029/92JC01511.

Emerson, S., and J. Hedges (2008), *Chemical Oceanography and the Marine Carbon Cycle*, Cambridge Univ. Press, Cambridge, U. K., and New York.

Erickson, D. J., C. Seuzaret, W. C. Keene, and S. L. Gong (1999), A general circulation model based calculation of HCl and ClNO2 production from sea salt dechlorination: Reactive Chlorine Emissions Inventory, *J. Geophys. Res.*, *104*(D7), 8347–8372, doi:10.1029/98JD01384.

Erlick, C., L. M. Russell, and V. Ramaswamy (2001), A microphysics-based investigation of the radiative effects of aerosol-cloud interactions for two MAST Experiment case studies, *J. Geophys. Res.*, *106*(D1), 1249–1269, doi:10.1029/2000JD900567.

Facchini, M. C., et al. (2008a), Primary submicron marine aerosol dominated by insoluble organic colloids and aggregates, *Geophys. Res. Lett.*, *35*, L17814, doi:10.1029/2008GL034210.

Facchini, M. C., et al. (2008b), Important source of marine secondary organic aerosol from biogenic amines, *Environ. Sci. Technol.*, *42*(24), 9116–9121.

Facchini, M. C., M. Rinaldi, S. Decesari, and S. Fuzzi (2010), Marine organic aerosol and biological oceanic activity, *Chem. Eng.*, *22*, 107–112.

Frossard, A. A., and L. M. Russell (2012), Removal of Sea Salt Hydrate Water from Seawater-Derived Samples by Dehydration, *Environ. Sci. Technol.*, *46*(24), 13,326–13,333, doi:10.1021/es3032083.

Frossard, A. A., P. M. Shaw, L. M. Russell, J. H. Kroll, M. R. Canagaratna, D. R. Worsnop, P. K. Quinn, and T. S. Bates (2011), Springtime Arctic haze contributions of submicron organic particles from European and Asian combustion sources, *J. Geophys. Res.*, *116*, D05205, doi:10.1029/2010JD015178.

Frossard, A. A., L. M. Russell, P. Massoli, T. S. Bates, and P. K. Quinn (2014), Side-by-side comparison of four techniques explains the apparent differences in the organic composition of generated and ambient marine aerosol particles, *Aerosol Sci. Technol.*, *48*(3), v–x, doi:10.1080/02786826.2013.879979.

Fu, P. Q., K. Kawamura, and K. Miura (2011), Molecular characterization of marine organic aerosols collected during a round-the-world cruise, *J. Geophys. Res.*, *116*, D13302, doi:10.1029/2011JD015604.

Fu, P. Q., K. Kawamura, J. Chen, B. Charriere, and R. Sempere (2013), Organic molecular composition of marine aerosols over the Arctic Ocean in summer: Contributions of primary emission and secondary aerosol formation, *Biogeosciences*, *10*(2), 653–667, doi:10.5194/bg-10-653-2013.

Fuentes, E., H. Coe, D. Green, G. de Leeuw, and G. McFiggans (2010), Laboratory-generated primary marine aerosol via bubble-bursting and atomization, *Atmos. Meas. Tech.*, *3*(1), 141–162.

Gantt, B., N. Meskhidze, M. C. Facchini, M. Rinaldi, D. Ceburnis, and C. D. O'Dowd (2011), Wind speed dependent size-resolved parameterization for the organic mass fraction of sea spray aerosol, *Atmos. Chem. Phys.*, *11*(16), 8777–8790.

Gao, Q., C. Leck, C. Rauschenberg, and P. A. Matrai (2012), On the chemical dynamics of extracellular polysaccharides in the high Arctic surface microlayer, *Ocean Sci.*, *8*, 401–418, doi:10.5194/os-8-401-2012.

Guzman-Morales, J., et al. (2013), Estimated Contributions of Primary and Secondary Organic Aerosol from Fossil Fuel Combustion during the CalNex and Cal-Mex Campaigns, *Atmos. Environ.*, *88*, 330–340.

Hansell, D. A. (2013), Recalcitrant Dissolved Organic Carbon Fractions, *Annu. Rev. Mar. Sci.*, *5*(5), 421–445, doi:10.1146/annurev-marine-120710-100757.

Hawkins, L. N., and L. M. Russell (2010), Polysaccharides, Proteins, and Phytoplankton Fragments: Four Chemically Distinct Types of Marine Primary Organic Aerosol Classified by Single Particle Spectromicroscopy, *Adv. Meteorol.*, *14*, doi:10.1155/2010/612132.

Hawkins, L. N., L. M. Russell, D. S. Covert, P. K. Quinn, and T. S. Bates (2010), Carboxylic acids, sulfates, and organosulfates in processed continental organic aerosol over the southeast Pacific Ocean during VOCALS-REx 2008, *J. Geophys. Res.*, *115*, D13201, doi:10.1029/2009JD013276.

Hoffman, E. J., and R. A. Duce (1976), Factors influencing the organic carbon content of marine aerosols: A laboratory study, *J. Geophys. Res.*, *81*(21), 3667–3670, doi:10.1029/JC081i021p03667.

Holland, H. D. (1978), *The Chemistry of the Atmosphere and Oceans*, pp. 154, Jonh Wiley, York New.

Hultin, K. A. H., E. D. Nilsson, R. Krejci, E. M. Martensson, M. Ehn, A. Hagstrom, and G. de Leeuw (2010), In situ laboratory sea spray production during the Marine Aerosol Production 2006 cruise on the northeastern Atlantic Ocean, *J. Geophys. Res.*, *115*, D06201, doi:10.1029/2009JD012522.

Kawamura, K., and R. B. Gagosian (1987), Implications of omega-oxocarboxylic acids in the remote marine atmosphere for photooxidation of unsaturated fatty-acids, *Nature*, *325*(6102), 330–332, doi:10.1038/325330a0.

Kawamura, K., and F. Sakaguchi (1999), Molecular distributions of water soluble dicarboxylic acids in marine aerosols over the Pacific Ocean including tropics, *J. Geophys. Res.*, *104*(D3), 3501–3509, doi:10.1029/1998JD100041.

Keene, W. C., R. Sander, A. A. P. Pszenny, R. Vogt, P. J. Crutzen, and J. N. Galloway (1998), Aerosol pH in the marine boundary layer: A review and model evaluation, *J. Aerosol Sci.*, *29*(3), 339–356, doi:10.1016/s0021-8502(97)10011-8.

Keene, W. C., et al. (2007), Chemical and physical characteristics of nascent aerosols produced by bursting bubbles at a model air-sea interface, *J. Geophys. Res.*, *112*, D21202, doi:10.1029/2007JD008464.

King, S. M., A. C. Butcher, T. Rosenoern, E. Coz, K. I. Lieke, G. de Leeuw, E. D. Nilsson, and M. Bilde (2012), Investigating primary marine aerosolproperties: CCN activity of sea salt and mixed inorganic–organic particles, *Environ. Sci. Technol.*, *46*(19), doi:10.1021/es300574u.

Kuhn, L. P. (1950), Infrared spectra of carbohydrates, *Anal. Chem.*, *22*(2), 276–283, doi:10.1021/ac60038a015.

Kuznetsova, M., C. Lee, and J. Aller (2005), Characterization of the proteinaceous matter in marine aerosols, *Mar. Chem.*, *96*(3–4), 359–377, doi:10.1016/j.marchem.2005.03.007.

Leck, C., and E. K. Bigg (2005), Biogenic particles in the surface microlayer and overlaying atmosphere in the central Arctic Ocean during summer, *Tellus B*, *57*, 305–316, doi:10.1111/j.1600-0889.2005.00148x.

Leck, C., and E. K. Bigg (2008), Comparison of sources and nature of the tropical aerosol with the summer high Arctic aerosol, *Tellus Ser. A B*, *60*(1), 118–126, doi:10.1111/j.1600-0889.2007.00315.x.

Leck, C., Q. Gao, F. Mashayekhy Rad, and U. Nilsson (2013), Size-resolved atmospheric particulate polysaccharides in the high summer Arctic, *Atmos. Chem. Phys.*, *13*, 12,573–12,588, doi:10.5194/acp-13-12573-2013.

Lewis, E. R., and S. E. Schwartz (2004), *Sea Salt Aerosol Production: Mechanisms, Methods, Measurements, and Models - A Critical Review*, AGU, Washington, D. C.

Liu, S., D. A. Day, J. E. Shields, and L. M. Russell (2011), Ozone-driven daytime formation of secondary organic aerosol containing carboxylic acid groups and alkane groups, *Atmos. Chem. Phys.*, *11*(16), 8321–8341, doi:10.5194/acp-11-8321-2011.

Long, M. S., W. C. Keene, D. J. Kieber, A. A. Frossard, L. M. Russell, J. R. Maben, J. D. Kinsey, P. K. Quinn, and T. S. Bates (2014), Light-enhanced primary marine aerosol production from biologically productive seawater, *Geophys. Res. Lett.*, *41*, 2661–2670, doi:10.1002/2014GL059436.

Maria, S. F., L. M. Russell, B. J. Turpin, and R. J. Porcja (2002), FTIR measurements of functional groups and organic mass in aerosol samples over the Caribbean, *Atmos. Environ.*, *36*(33), 5185–5196.

Maria, S. F., L. M. Russell, B. J. Turpin, R. J. Porcja, T. L. Campos, R. J. Weber, and B. J. Huebert (2003), Source signatures of carbon monoxide and organic functional groups in Asian Pacific Regional Aerosol Characterization Experiment (ACE-Asia) submicron aerosol types, *J. Geophys. Res.*, *108*(D23), 8637, doi:10.1029/2003JD003703.

Martensson, E. M., E. D. Nilsson, G. de Leeuw, L. H. Cohen, and H. C. Hansson (2003), Laboratory simulations and parameterization of the primary marine aerosol production, *J. Geophys. Res.*, *108*(D9), 4297, doi:10.1029/2002JD002263.

Mathlouthi, M., and J. L. Koenig (1986), Vibrational-spectra of carbohydrates, *Adv. Carbohydrate Chem. Biochem.*, *44*, 7–89.

Matsumoto, K., and M. Uematsu (2005), Free amino acids in marine aerosols over the western North Pacific Ocean, *Atmos. Environ.*, *39*(11), 2163–2170, doi:10.1016/j.atmosenv.2004.12.022.

Meskhidze, N., and A. Nenes (2006), Phytoplankton and cloudiness in the Southern Ocean, *Science*, *314*(5804), 1419–1423, doi:10.1126/science.1131779.

Mochida, M., Y. Kitamori, K. Kawamura, Y. Nojiri, and K. Suzuki (2002), Fatty acids in the marine atmosphere: Factors governing their concentrations and evaluation of organic films on sea-salt particles, *J. Geophys. Res.*, *107*(D17), 4325, doi:10.1029/2001JD001278.

Modini, R. L., L. M. Russell, G. B. Deane, and M. D. Stokes (2013), Effect of soluble surfactant on bubble persistence and bubble-produced aerosol particles, *J. Geophys. Res. Atmos.*, *118*, 1388–1400, doi:10.1002/jgrd.50186.

Naumann, D., G. Barnickel, H. Bradaczek, H. Labischinski, and P. Giesbrecht (1982), Infrared-spectroscopy, a tool for probing bacterial peptidoglycan - potentialities of infrared-spectroscopy for cell-wall analytical studies and rejection of models based on crystalline chitin, *Eur. J. Biochem.*, *125*(3), 505–515, doi:10.1111/j.1432-1033.1982.tb06711.x.

Nilsson, E. D., U. Rannik, E. Swietlicki, C. Leck, P. P. Aalto, J. Zhou, and M. Norman (2001), Turbulent aerosol fluxes over the Arctic Ocean 2. Wind-driven sources from the sea, *J. Geophys. Res.*, *106*(D23), 32,139–32,154, doi:10.1029/2000JD900747.

O'Dowd, C. D., and G. De Leeuw (2007), Marine aerosol production: A review of the current knowledge, *Philoso. Trans. R. Soc. A-Mathematical Physical and Engineering Sciences*, *365*(1856), 1753–1774, doi:10.1098/rsta.2007.2043.

O'Dowd, C. D., et al. (2002), A dedicated study of New Particle Formation and Fate in the Coastal Environment (PARFORCE): Overview of objectives and achievements, *J. Geophys. Res.*, *107*(D19), 8108, doi:10.1029/2001JD000555.

O'Dowd, C. D., M. C. Facchini, F. Cavalli, D. Ceburnis, M. Mircea, S. Decesari, S. Fuzzi, Y. J. Yoon, and J. P. Putaud (2004), Biogenically driven organic contribution to marine aerosol, *Nature*, *431*(7009), 676–680, doi:10.1038/nature02959.

Oppo, C., S. Bellandi, N. D. Innocenti, A. M. Stortini, G. Loglio, E. Schiavuta, and R. Cini (1999), Surfactant components of marine organic matter as agents for biogeochemical fractionation and pollutant transport via marine aerosols, *Mar. Chem.*, *63*(3–4), 235–253, doi:10.1016/s0304-4203(98)00065-6.

Orellana, M. V., and P. Verdugo (2003), Ultraviolet radiation blocks the organic carbon exchange between the dissolved phase and the gel phase in the ocean, *Limnol. Oceanogr.*, *48*(4), 1618–1623.

Orellana, M. V., P. A. Matrai, C. Leck, C. D. Rauschenberg, A. M. Lee, and E. Coz (2011), Marine microgels as a source of cloud condensation nuclei in the high Arctic, *Proc. Natl. Acad. Sci. U.S.A.*, *108*(33), 13,612–13,617.

Ovadnevaite, J., C. O'Dowd, M. Dall'Osto, D. Ceburnis, D. R. Worsnop, and H. Berresheim (2011), Detecting high contributions of primary organic matter to marine aerosol: A case study, *Geophys. Res. Lett.*, *38*, L02807, doi:10.1029/2010GL046083.

Pavia, D. L., G. M. Lapman, and G. S. Kriz (2001), *Introduction to Spectroscopy*, 3rd ed., Harcourt College Publishers, Fort Worth, Tex.

Pszenny, A. A. P., W. C. Keene, D. J. Jacob, S. Fan, J. R. Maben, M. P. Zetwo, M. Springeryoung, and J. N. Galloway (1993), Evidence of inorganic chlorine gases other than hydrogen-chloride in marine surface air, *Geophys. Res. Lett.*, *20*(8), 699–702, doi:10.1029/93GL00047.

Quinn, P. K., D. J. Coffman, V. N. Kapustin, T. S. Bates, and D. S. Covert (1998), Aerosol optical properties in the marine boundary layer during the First Aerosol Characterization Experiment (ACE 1) and the underlying chemical and physical aerosol properties, *J. Geophys. Res.*, *103*(D13), 16,547–16,563, doi:10.1029/97JD02345.

Quinn, P. K., T. S. Bates, K. S. Schultz, D. C. Coffman, A. A. Frossard, L. M. Russell, W. C. Keene, and D. J. Kieber (2014), "Empirical constraints on modeling the organic matter enrichment in nascent sea spray aerosol," *Nat. Geosci.*, *7*, 228–232, doi:10.1038/NGEO2092.

Randles, C. A., L. M. Russell, and V. Ramaswamy (2004), Hygroscopic and optical properties of organic sea salt aerosol and consequences for climate forcing, *Geophys. Res. Lett.*, *31*, L16108, doi:10.1029/2004GL020628.

Redfield, A. C. (1934), On the proportions of organic derivatives in sea water and their relation to the composition of plankton, in *James Johnstone Memorial*, edited by R. J. Daniel, pp. 176–171, Univ. Press of Liverpool, Liverpool, U. K.

Rinaldi, M., S. Decesari, E. Finessi, L. Giulianelli, C. Carbone, S. Fuzzi, C. D. O'Dowd, D. Ceburnis, and M. C. Facchini (2010), Primary and secondary organic marine aerosol and oceanic biological activity: Recent results and new perspectives for future studies, *Adv. Meteorol.*, *10*, 1–11, doi:10.1155/2010/310682.

Rogge, W. F., M. A. Mazurek, L. M. Hildemann, G. R. Cass, and B. R. T. Simoneit (1993), Quantification of urban organic aerosols at a molecular-level - identification, abundance and seasonal-variation, *Atmos. Environ. Part A-General Topics*, *27*(8), 1309–1330.

Russell, L. M. (2003), Aerosol organic-mass-to-organic-carbon ratio measurements, *Environ. Sci. Technol.*, *37*(13), 2982–2987, doi:10.1021/es026123w.

Russell, L. M., S. Takahama, S. Liu, L. N. Hawkins, D. S. Covert, P. K. Quinn, and T. S. Bates (2009), Oxygenated fraction and mass of organic aerosol from direct emission and atmospheric processing measured on the R/V Ronald Brown during TEXAQS/GoMACCS 2006, *J. Geophys. Res.*, *114*, D00F05, doi:10.1029/2008JD011275.

Russell, L. M., L. N. Hawkins, A. A. Frossard, P. K. Quinn, and T. S. Bates (2010), Carbohydrate-like composition of submicron atmospheric particles and their production from ocean bubble bursting, *Proc. Natl. Acad. Sci. U.S.A.*, *107*(15), 6652–6657, doi:10.1073/pnas.0908905107.

Russell, L. M., et al. (2013), Eastern Pacific Emitted Aerosol Cloud Experiment, *Bull. Am. Meteorol. Soc.*, *94*(5), 709 −729, doi:10.1175/bams-d-12-00015.1.

Satsumabayashi, H., H. Kurita, Y. Yokouchi, and H. Ueda (1990), Photochemical formation of particulate dicarboxylic-acids under long-range transport in central Japan, *Atmos. Environ. Part A-General Topics*, *24*(6), 1443–1450, doi:10.1016/0960-1686(90)90053-p.

Schmitt-Kopplin, P., et al. (2012), Dissolved organic matter in sea spray: A transfer study from marine surface water to aerosols, *Biogeosciences*, *9*(4), doi:10.5194/bg-9-1571-2012.

Sciare, J., O. Favez, R. Sarda-Esteve, K. Oikonomou, H. Cachier, and V. Kazan (2009), Long-term observations of carbonaceous aerosols in the Austral Ocean atmosphere: Evidence of a biogenic marine organic source, *J. Geophys. Res.*, *114*D15302, doi:10.1029/2009JD011998.

Sellegri, K., C. D. O'Dowd, Y. J. Yoon, S. G. Jennings, and G. de Leeuw (2006), Surfactants and submicron sea spray generation, *J. Geophys. Res.*, *111*, D22215, doi:10.1029/2005JD006658.

Shank, L. M., S. Howell, A. D. Clarke, S. Freitag, V. Brekhovskikh, V. Kapustin, C. McNaughton, T. Campos, and R. Wood (2012), Organic matter and non-refractory aerosol over the remote Southeast Pacific: Oceanic and combustion sources, *Atmos. Chem. Phys.*, *12*(1), doi:10.5194/acp-12-557-2012.

Takahama, S., S. Gilardoni, L. M. Russell, and A. L. D. Kilcoyne (2007), Classification of multiple types of organic carbon composition in atmospheric particles by scanning transmission X-ray microscopy analysis, *Atmos. Environ.*, *41*(40), 9435–9451, doi:10.1016/j.atmosenv.2007.08.051.

Takahama, S., S. Liu, and L. M. Russell (2010), Coatings and clusters of carboxylic acids in carbon-containing atmospheric particles from spectromicroscopy and their implications for cloud-nucleating and optical properties, *J. Geophys. Res.*, *115*, D01202, doi:10.1029/2009JD012622.

Takahama, S., A. Johnson, and L. M. Russell (2013), Quantification of carboxylic and carbonyl functional groups in organic aerosol infrared absorbance spectra, *Aerosol Sci. Technol.*, doi:10.1080/02786826.2012.752065.

Turekian, V. C., S. A. Macko, and W. C. Keene (2003), Concentrations, isotopic compositions, and sources of size-resolved, particulate organic carbon and oxalate in near-surface marine air at Bermuda during spring, *J. Geophys. Res.*, *108*(D5), *4157*, doi:10.1029/2002JD002053.

Venyaminov, S. Y., and N. N. Kalnin (1990), Quantitative IR spectrophotometry of peptide compounds in water (H2O) solutions.1 Spectral parameters of amino-acid residue absorption-bands, *Biopolymers*, *30*(13–14), 1243–1257, doi:10.1002/bip.360301309.

Verdugo, P., A. L. Alldredge, F. Azam, D. L. Kirchman, U. Passow, and P. H. Santschi (2004), The oceanic gel phase: A bridge in the DOM-POM continuum, *Mar. Chem.*, *92*(1–4), 67–85, doi:10.1016/j.marchem.2004.06.017.

Ward, J. H. (1963), Hierarchical grouping to optimize an objective function, *J. Am. Stat. Assoc.*, *58*(301), doi:10.2307/2282967.

Williams, P. M., A. F. Carlucci, S. M. Henrichs, E. S. Vanvleet, S. G. Horrigan, F. M. H. Reid, and K. J. Robertson (1986), Chemical and microbiological studies of sea-surface films in the southern gulf of California and off the west-coast of Baja-California, *Mar. Chem.*, *19*(1), 17–98, doi:10.1016/0304-4203(86)90033-2.

Wonaschutz, A., et al. (2013), Hygroscopic properties of smoke-generated organic aerosol particles emitted in the marine atmosphere, *Atmos. Chem. Phys.*, *13*, 9819–9835.

Wurl, O., and M. Holmes (2008), The gelatinous nature of the sea-surface microlayer, *Mar. Chem.*, *110*(1–2), 89–97, doi:10.1016/j.marchem.2008.02.009.

Wurl, O., E. Wurl, L. Miller, K. Johnson, and S. Vagle (2011), Formation and global distribution of sea-surface microlayers, *Biogeosciences*, *8*(1), 121–134, doi:10.5194/bg-8-121-2011.

Yoon, Y. J., et al. (2007), Seasonal characteristics of the physicochemical properties of North Atlantic marine atmospheric aerosols, *J. Geophys. Res.*, *112*, D04206, doi:10.1029/2005JD007044.

Zhang, Q., D. R. Worsnop, M. R. Canagaratna, and J. L. Jimenez (2005), Hydrocarbon-like and oxygenated organic aerosols in Pittsburgh: insights into sources and processes of organic aerosols, *Atmos. Chem. Phys.*, *5*, 3289–3311.

Zhou, X. L., A. J. Davis, D. J. Kieber, W. C. Keene, J. R. Maben, H. Maring, E. E. Dahl, M. A. Izaguirre, R. Sander, and L. Smoydzyn (2008), Photochemical production of hydroxyl radical and hydroperoxides in water extracts of nascent marine aerosols produced by bursting bubbles from Sargasso seawater, *Geophys. Res. Lett.*, *35*, L20803, doi:10.1029/2008GL035418.

Zutic, V., B. Cosovic, E. Marcenko, N. Bihari, and F. Krsinic (1981), Surfactant production by marine-phytoplankton, *Mar. Chem.*, *10*(6), 505–520, doi:10.1016/0304-4203(81)90004-9.